Check for updates

21698996, ja, Downloaded from https://agupubs.onlinelibrary.wiley.com/doi/10.1029/2021JD035476 by University Of Oslo Central 340, Wiley Online Library on [21/10/2022]. See the Terms and Conditions (https://onlinelibrary.wiley.com/terms-and-conditions) on Wiley Online Library for rules of use; OA articles are governed by the applicable Creative Commons License

Accepted Article

Disentangling Aerosol and Cloud effects on Dimming and Brightening in Observations and CMIP6

I.R. Julsrud[1,2,3*], T. Storelvmo[2], M. Schulz[3,2], K.O. Moseid[3,2], M. Wild[4]

[1] Norwegian Institute for Air Research (NILU), Kjeller, Norway

[2] University of Oslo (UiO), Oslo, Norway

[3] Norwegian Meteorological Institute (MET Norway), Oslo, Norway

[4] ETH Zurich, Institute for Atmospheric and Climate Science, Zurich, Switzerland

Corresponding author: Ingeborg Rian Julsrud (ingeborg.rj@gmail.com)

* Much of the scientific work presented in this paper was conducted as part of the first author's master's degree at UiO (2020); this manuscript was written during her time at NILU.

Key Points:

- This study supports evidence that dimming and brightening trends between 1961 and 2014 in China, Japan, Europe and the United States were caused by variations in aerosol- and aerosol precursor emissions, and not by cloud cover changes.
- Results confirm and reinforce previous indications that CMIP6 simulations are able to reproduce SSR trends observed in Europe, but not in China, Japan and the United States.

Abstract

Periods of dimming and brightening have been recorded in observational datasets of surface solar radiation (SSR) between the mid-20th century and present day. Atmospheric components affect SSR, including aerosols and clouds, though studies disagree somewhat about the relative effect of each component in different regions. Current Earth system models (ESMs) are unable to simulate observed trends in SSR. This study includes an investigation into observed SSR variations between 1961 and 2014 and an evaluation of the effects of cloud cover variations and impacts of aerosol extinction, using timeseries of SSR and cloud cover from in-situ measurements. Historical simulations by 42 ESMs participating in the Coupled Model Intercomparison Project Phase 6 (CMIP6) have also been studied and compared to observations. The observational study indicates that cloud cover has had a dampening effect on the variations of SSR and that emissions of aerosol and aerosol precursors are the main cause of the general trends in observed SSR in four regions—China, Japan, Europe and the United States—during 1961-2014. The study of simulated SSR in CMIP6 yields the conclusion that current ESMs remain unable to simulate the magnitude of observed dimming and brightening in China, Japan and the United States, but that the European SSR trends between 1961 and 2014 are fairly well reproduced in the ESMs. A rough quantification of the regional surface radiation extinction efficiency of aerosol and precursor emissions in the simulations is found to agree with observed values in Europe, but not in the other three regions.

Plain Language Summary

Measurements of incoming sunlight at the Earth's surface between the 1960s and the 1980s show a substantial downward trend globally, and between the 1980s and the 2000s an upward trend has followed, albeit weaker. These two trends are often called *dimming* and *brightening*, respectively. The reasons for dimming and brightening are not clear, although

This article has been accepted for publication and undergone full peer review but has not been through the copyediting, typesetting, pagination and proofreading process, which may lead to differences between this version and the Version of Record. Please cite this article as doi: 10.1029/2021JD035476.

This article is protected by copyright. All rights reserved.

evidence supports the role of atmospheric components, prominently aerosol emissions and clouds; changes in aerosol emissions and clouds can cause changes in incoming sunlight at the surface because of their ability to absorb or reflect sunlight on its way through the atmosphere. In this study, measurements of incoming sunlight at the surface are investigated and compared with simulations from state-of-the-art Earth system models. The study supports evidence that aerosol emission changes have been causal to observed regional dimming and brightening, and suggests that cloud cover changes have not caused the trends. The study also finds that Earth system models are unable to compute dimming and brightening trends in several regions, which may suggest that the models are not accurately reproducing the atmospheric processes that cause the trends.

1 Introduction

Globally since the mid-20th century, substantial variations have been recorded in the amount of incoming solar radiation at the surface (Ohmura & Lang, 1989; Russak, 1990; Stanhill & Moreshet, 1994; Stanhill & Kalma, 1995; Liepert & Kukla, 1997; Gilgen, et al., 1998; Stanhill & Cohen, 2001; Liepert, 2002; Wild, 2009, 2012, 2016; Wang, et al., 2012; Wild, et al., 2021; references therein). For the period 1950–1980, a widespread decrease in surface solar radiation (SSR) of on average about 4 W/m^2 was observed, now often referred to as "global dimming" or just "dimming", and since the 1980s, a regionally dependent slight increase in SSR has followed, aptly termed "brightening".

Evidence suggests that the luminosity of the sun has not exhibited trends that could be causal to the dimming and brightening trends (Willson & Mordvinov, 2003; Hoyt & Schatten, 1993). This indicates that changes internal to the atmosphere are the likely cause. A large body of evidence suggests that dimming and brightening were generally caused by changes in aerosol concentration in the atmosphere (Wild, 2012 and references therein). Other evidence suggests that cloud cover variations independent of aerosol presence have played a crucial role in the SSR trends regionally (e.g., Norris & Wild, 2009; Pfeifroth, et al., 2018; Long, et al., 2009). Thus far, consensus has not been reached regarding the relative roles of clouds and aerosols in the causation of the SSR trends (Wild, 2016), and this issue is therefore a focus of this study.

Aerosols have a substantial effect on the radiative transmissivity of the atmosphere (e.g., Ramanathan, et al., 2001; Myhre, et al., 2013; Boucher, 2015). Aerosols and their precursors (gaseous species that lead to the production of aerosols) enter the atmosphere as a result of both natural and anthropogenic emissions, and while some aerosols are fully formed upon emission, others form after emission upon precursor gases reacting with other atmospheric components. In this study, anthropogenic emissions of aerosols and aerosol precursors are studied. Important emissions in this regard are SO_2 (precursor), NH_3 (precursor), black carbon (aerosol), organic carbon (aerosol), NO_X (precursor) and NMVOC (precursor) (Boucher, et al., 2013; Naik, et al., 2021). The global emissions of aerosols and aerosol precursors have changed substantially during the dimming and brightening periods (Wild, 2012), but the development differs across regions (Streets, et al., 2006).

Clouds are the planet's most effective shield against sunlight, covering roughly two thirds of Earth's surface at any given time (Boucher, et al., 2013). The sign and magnitude of long-term trends in cloud cover are different between regions (Norris, et al., 2016), which means that the effect of cloud cover changes on SSR trends must also vary regionally.

In addition to aerosols and clouds being independent factors that affect SSR, they interact with each other (e.g., Ramanathan, et al., 2001; Myhre, et al., 2013; Boucher, 2015). Specifically, clouds' optical properties and lifetimes can change considerably because of aerosols, and an aerosol particle's atmospheric lifetime can be affected upon interaction with a cloud.

This article is protected by copyright. All rights reserved.

Accepted Article

21698996, ja, Downloaded from https://agupubs.onlinelibrary.wiley.com/doi/10.1029/2021JD035476 by University Of Oslo Central 340, Wiley Online Library on [21/10/2022]. See the Terms and Conditions (https://onlinelibrary.wiley.com/terms-and-conditions) on Wiley Online Library for rules of use; OA articles are governed by the applicable Creative Commons License

This complicated picture results in high uncertainty tied to aerosols and clouds in Earth system model (ESM) projections, and aerosols and clouds continue to contribute the largest uncertainty to modeling of the Earth's changing energy budget according to the 6th Assessment Report by the Intergovernmental Panel on Climate Change (Forster, et al., 2021). This is because the respective effects play an important role in the energy budget, while the mechanisms of their interactions are not well established and their properties vary at scales significantly smaller than those resolved in climate models.

These issues are specifically relevant for dimming and brightening because, thus far, ESMs have not been able to reproduce the magnitude of these SSR trends in historical experiments (Wild & Schmucki, 2011; Allen, et al., 2013; Storelvmo, et al., 2018; Moseid, et al., 2020). Since SSR represents a significant part of the Earth's energy budget and influences a variety of surface and atmospheric processes, it is essential to understand why the ESMs cannot reproduce the observed variations in SSR—indeed, this ESM shortcoming raises uncertainties about model projections for future climate change. Thus, this study attempts to disentangle the SSR effects of aerosol emissions from those of cloud cover in both observations and ESM output, in order to improve current understanding of the causes behind dimming and brightening.

2 Data

For the analysis in this study, both observational data and simulation output from Earth system models (ESMs) are included. In this section, the observational data will be introduced first, followed by a description of the ESM data.

2.1 GEBA and ngGEBA

The original Global Energy Balance Archive (GEBA) contains surface energy balance components measured at 2500 locations worldwide (Wild, et al., 2017), including measurements of SSR. Most SSR measurements included in GEBA are made with pyranometer instruments. While GEBA has an outstanding spatial coverage, a large fraction of the stations contain substantial temporal gaps during the dimming and brightening periods. To handle this, an altered version of GEBA is studied here instead, which has previously been included in two studies about dimming and brightening, namely Storelvmo, et al. (2018) and Moseid, et al. (2020). The altered GEBA SSR data contains exclusively complete timeseries between 1961 and 2014, and is dubbed "ngGEBA" (short for "no-gap GEBA") in the current study. Many GEBA stations' timeseries were omitted from this version of the dataset due to insufficient coverage. However, many incomplete SSR timeseries were instead filled and temporally expanded to cover the period 1961 to 2014 by using the machine learning method *random forest*; the method is described and evaluated in Leirvik & Yuan (2021). ngGEBA has 1487 full monthly datasets from between 1961 and 2014 globally, of which approximately 2/3 is generated through the random forest algorithm.

China is one of the regions of focus in this study, and therefore, recent literature regarding the veracity of the Chinese SSR data must be discussed. During the 1990s, there were substantial and widespread changes made to the ground-based network of SSR instruments in China. A large number of instruments were replaced in the early 1990s (Wang & Wild, 2016), and changes were made to instrument locations and the frequency of measurement. Wang & Wild (2016) proposed that these changes were the main cause of a certain reversal and exaggerated trend in the Chinese national average SSR series during the 1990s.

Yang, et al. (2018) created a homogenized version of the Chinese national SSR timeseries, assessing the homogeneity of Chinese SSR data from China Meteorological

This article is protected by copyright. All rights reserved.

Accepted Article

21698996, ja, Downloaded from https://agupubs.onlinelibrary.wiley.com/doi/10.1029/2021JD035476 by University Of Oslo Central 340, Wiley Online Library on [21/10/2022]. See the Terms and Conditions (https://onlinelibrary.wiley.com/terms-and-conditions) on Wiley Online Library for rules of use; OA articles are governed by the applicable Creative Commons License

Agency (CMA) weather stations using nearby surface sunshine duration data as reference. An adjusted version of the SSR timeseries appears in Figure 10 of Yang, et al. (2018), showing the national average SSR timeseries in its raw and adjusted form. Said figure clearly shows that the original timeseries' "jump" of 10 W/m^2 in the early 1990s seems to be an artifact, because the adjusted timeseries instead exhibits a levelling off during the 1990s and is followed by a slow dimming of ~2 W/m^2 until the early 2000s.

A similar 1990s "jump" is present in ngGEBA (studied herein), but a homogeneized version of ngGEBA in China has not been realized thus far. For the purpose of the analysis in this study, a crude attempt is made to match the Chinese ngGEBA SSR timeseries to that resulting from the homogenization performed by Yang, et al. (2018); the procedure to do so is simply to increase the ngGEBA SSR magnitude by adding +7 W/m^2 in the period 1961 to 1990.

2.2 CRU TS cloud percentage cover

CRU TS is a high-resolution (0.5° × 0.5°), gridded, monthly observational dataset covering land areas, excluding Antarctica (Harris & Osborn, 2020). The dataset contains values from 1901 and onward and includes, among other parameters, historical timeseries of cloud percentage cover. The cloud parameter is partially based on direct station observations of cloud cover, but it largely relies on proxy measurements of other observed variables such as sunshine duration measurements and daily temperature range (Harris, et al., 2014)2The CRU dataset is interpolated, and contains no gaps within its domain; the interpolation method is thoroughly described in Harris, et al. (2014). The completeness of the dataset allows for collocation with the ngGEBA stations (see Section 2.1) for the period 1961–2014.

The temporal coverage of CRU cloud cover is unique, containing monthly entries from 1901 and onward. Pre-satellite era, there are few alternatives to test CRU cloud cover against, and no comparison analyses exist to the knowledge of the authors. One satellite-era study covering the Iberian peninsula does indicate that CRU cloud cover is in disagreement with gridded satellite (ISCCP D2) and reanalysis (ERA-40) data (Calbó & Sanchez-Lorenzo, 2009). However, satellite measurements do not extend far enough back to be sufficient for the analysis in this study, and cloud cover data from reanalyses are a model product and not fitted for observational analysis.

2.3 CEDS emissions

CEDS (Community Emissions Data System) emission data is a widely used gridded global emission dataset of 50 km nominal resolution, which includes estimates of historical emissions of gases and aerosols, along with future projections of emissions (Smith, et al., 2015). The data is used in the Coupled Model Intercomparison Project Phase 6, CMIP6 (Eyring, et al., 2016; see also Section 2.4), serving as the input data for the participating Earth system models (ESMs). In this study, CEDS anthropogenic aerosol/precursor emissions are compared with observed and modelled SSR and cloud data. The emissions included are anthropogenic emissions of SO_2, NH_3, black carbon, organic carbon, NO_X and NMVOC (non-methane volatile organic compounds). These species are cited as the main anthropogenically sourced aerosol/precursor emissions in the IPCC's sixth assessment report (Naik, et al., 2021).

A simple sum of the mass emissions of these species is dubbed "aerosol/precursor emissions" in this study, and this sum gives a rough estimate of the total emitted aerosols/precursors without considering differences in SSR extinction efficiency per mass across species. The aerosol/precursor emissions normalized to the horizontal area of each

This article is protected by copyright. All rights reserved.

Accepted Article

21698996, ja, Downloaded from https://agupubs.onlinelibrary.wiley.com/doi/10.1029/2021JD035476 by University Of Oslo Central 340, Wiley Online Library on [21/10/2022]. See the Terms and Conditions (https://onlinelibrary.wiley.com/terms-and-conditions) on Wiley Online Library for rules of use; OA articles are governed by the applicable Creative Commons License

respective region of study; i.e., timeseries of total emissions from one region (e.g., China) is divided by the area of the region.

Two versions of the CEDS emission data are included herein, one for the CMIP6 analysis and one for the observational analysis:

- *CMIP6 CEDS*, the emission forcing data used for CMIP6 (Smith, et al., 2015), is studied when analyzing effects of aerosol/precursor emissions on ESM simulations, because CMIP6 CEDS is the simulations' input emission data.
- *2020 CEDS*, a newer version of CEDS emission data published in 2020 (O'Rourke, et al., 2020) is compared to observational data; this emission inventory has not been used as input in the CMIP6 historical experiments; however, arguably it is a more updated and accurate version than the input emissions.

The differences between the two datasets can be found in the release notes of 2020 CEDS (O'Rourke, et al., 2020). Differences that are relevant for the current study include the decrease of Chinese emissions of organic and black carbon after 2000 in 2020 CEDS, where CMIP6 CEDS exhibits an increase. The post-2000 emissions from China were investigated for CMIP6 CEDS in Wang, et al. (2021) and references therein; Wang, et al. (2021) argue that, between 2006 and 2014, CMIP6 CEDS exhibits an increase in total aerosol emissions, whereas an allegedly more trustworthy dataset from Peking University exhibits a decrease. A post-2000 emission decrease is captured by the 2020 CEDS dataset in emissions of carbon species.

2.4 CMIP6

To evaluate ESM performance by comparison with the observed SSR and cloud cover data, this study includes output from the CMIP6 historical experiment. These historical simulations are initiated from preindustrial control simulations, and are forced with historical data, including concentrations of various atmospheric species and emissions. The simulations start in 1850 and end in 2014, but for the purpose of this study, the years 1961–2014 were studied. Historical simulations from 42 ESMs are included here, and while some model centers do offer several ensemble members (experiments with differently perturbed initial conditions), one ensemble member from each model is included. The names and horizontal resolutions of the ESMs are provided in Table A (Appendix A). The variables included in this study are *rsdt* (insolation at the top of the atmosphere), *rsds* (surface solar radiation), *rsdscs* (clear-sky surface solar radiation) and *clt* (cloud cover total).

3 Methods

The analysis in this study is focused around four regions, and Section 3.1 describes the way in which these are selected and delineated from the data presented in Section 2. The method which isolates cloud cover-caused SSR variability from other extinction is subsequently introduced in Section 3.2.

3.1 Regions

The regions that are included in this study are China, Japan, Europe (omitting Russia) and the United States. Figure 1 shows the distribution of ngGEBA stations, and Table 1 shows the number of stations in each region. Cloud cover observations and CMIP6 output data is collocated to these station locations. The regions are chosen due to the relatively high number of ngGEBA stations located in each. Russia is left out from the European region because the density of stations is too low there to argue that the average of stations can represent the area.

This article is protected by copyright. All rights reserved.

Accepted Article

21698996, ja, Downloaded from https://agupubs.onlinelibrary.wiley.com/doi/10.1029/2021JD035476 by University Of Oslo Central 340, Wiley Online Library on [21/10/2022]. See the Terms and Conditions (https://onlinelibrary.wiley.com/terms-and-conditions) on Wiley Online Library for rules of use; OA articles are governed by the applicable Creative Commons License

Accepted Article

Some coverage issues do remain within the chosen regions. For instance, ngGEBA station density is low in western China and in Scandinavia, but these regions are not omitted from the analysis.

As stated, emission data are not collocated to the ngGEBA stations, but are rather aggregated as a sum of all aerosol/precursor emissions (see Section 2.3) in the region. A normalization "per area" is performed on the CEDS data to facilitate comparison between regions. The area of Alaska is omitted from the United States due to very few ngGEBA stations, low emissions and large relative area.

The following areas are used for emission normalization:

- China: 9.597×10^{12} m^2
- Japan: 3.77915×10^{11} m^2
- Europe without Russia: 6.1848×10^{12} m^2
- United States without Alaska: 8.115×10^{12} m^2

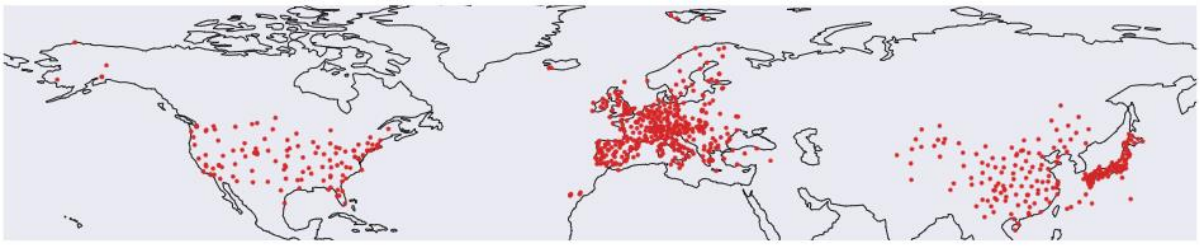

Figure 1: Overview of the distribution of ngGEBA stations studied herein. ngGEBA is presented in Section 2.1. The station records have been complemented using a machine learning algorithm, random forests.

Table 1**:** The number of ngGEBA stations located in each of the regions of focus in this study. The number of stations in Russia and Alaska are already subtracted in the ”ngGEBA stns.” column for Europe and the United States.

Region	ngGEBA stns.	To be noted
China	119	
Japan	100	
Europe	471	Not incl. Russia
United States	122	Not incl. Alaska

Unfortunately, it is not a straightforward task to perform a completely fair normalization, since emissions are not evenly distributed across the entire areas of, e.g., countries. It must therefore be understood that large areas with zero emissions are included in the areas used for normalization—this is the case in China, Europe and the United States. Japan, on the other hand, being an island country and decidedly the smallest region studied, loses a large fraction of its emissions to the surroundings. Thus, for Japan, normalized emissions may give an inflated impression of the total aerosol emissions. That said, the current study investigates temporal changes in emissions; a completely fair normalization is therefore not necessary for the objectives herein.

3.2 Computing “no-cloud SSR”

To separate the effects on SSR of cloud cover variations from those of other radiatively effective components such as aerosols, a “no-cloud SSR” timeseries from observations is created for the analysis in this study. For clarity, it is important to distinguish between this calculated no-cloud SSR and *clear-sky SSR* provided by ESMs, since these are different, which will be further discussed below.

This article is protected by copyright. All rights reserved.

21698996, ja, Downloaded from https://agupubs.onlinelibrary.wiley.com/doi/10.1029/2021JD035476 by University Of Oslo Central 340, Wiley Online Library on [21/10/2022]. See the Terms and Conditions (https://onlinelibrary.wiley.com/terms-and-conditions) on Wiley Online Library for rules of use; OA articles are governed by the applicable Creative Commons License

No-cloud SSR ($E_{no-cloud}$) is computed for a given month and station location from timeseries of all-sky SSR ($E_{all-sky}$) and cloud cover fraction (CLD). The procedure is simple: $E_{all-sky}$ is assumed made up of the SSR during cloudy conditions (E_{cloudy}) and the SSR during non-cloudy conditions ($E_{no-cloud}$), where the CLD timeseries determines the temporal fraction of each condition:

$$E_{all-sky} = E_{cloudy} \times CLD + E_{no-cloud} \times (1 - CLD) \qquad (1)$$

The equation can then be solved for $E_{no-cloud}$:

$$E_{no-cloud} = \frac{E_{all-sky} - E_{cloudy} \times CLD}{1 - CLD} \qquad (2)$$

The only unknown on the right-hand side of Equation 2 is E_{cloudy}, which should represent the SSR during cloudy conditions. "Cloudy conditions" must here be understood as a situation in which the sun is hidden behind a cloud as observed from the SSR instrument on Earth; a timeseries of CLD with a monthly resolution can reasonably be assumed to represent the fraction of time when the sun is covered by a cloud.

As a first analysis step, it is assumed that E_{cloudy} takes a characteristic constant value, representing average SSR during cloudy conditions. Further discussion on this assumption is included below.

It was previously stated that one must distinguish between no-cloud SSR and clear-sky SSR, and as will be showed later in this article, these two SSR variants can differ significantly. One noteable difference is that changes to the SSR during cloudy conditions, unrelated to cloud cover changes, will be captured in no-cloud SSR. This is because the computation of no-cloud SSR includes the variable E_{cloudy}, which is not a directly observed parameter in this analysis, and the variable must be set by the data analyst. One major cause of changes in SSR during cloudy conditions is of course aerosol-cloud interactions, which can result in altered cloud optical properties without necessarily affecting cloud cover (Twomey, 1977; Boucher, 2015). Also, cloud optical properties change depending on weather- and climate factors such as cloud height, altitude and humidity (Matuszko, 2012), and variations in these cloud properties will still influence no-cloud SSR. It must also be noted that the computation of no-cloud SSR depends on the accuracy of both the SSR dataset and the cloud cover dataset, meaning that uncertainty from both datasets is introduced when computing no-cloud SSR. Only annual- and decadal averages are considered in this study, so short-term and seasonal factors are averaged out of consideration. Section 4.2 explores various constants for E_{cloudy} and the sensitivity of no-cloud SSR to the value of this constant.

The choice of E_{cloudy} in Equation 2 is not trivial, and should therefore be explored. Matuszko (2012) presents a set of measured values that relate cloud area fraction with SSR, depending on the angular position of the Sun above the horizon. Matuszko (2012)'s values are generalizations computed from measurements between 2004 and 2007 in Krakow, Poland. Assuming average annual daytime solar zenith angle lies between 60° and 70° in Krakow (Cronin, 2014), the relevant average annual E_{cloudy} according to Matuszko (2012) is 109 W/m^2.

In order to extrapolate the observed Krakow-value to represent the average annual E_{cloudy} in the regions of focus here, a scaling was performed, dependent upon the annual average incoming solar radiation at the top of the atmosphere in each region. Gridded values of insolation at the top of the atmosphere (TOA) were collocated to the latitude and longitude of Krakow and to the ngGEBA stations in each region and annual averages were computed

This article is protected by copyright. All rights reserved.

Accepted Article

21698996, ja, Downloaded from https://agupubs.onlinelibrary.wiley.com/doi/10.1029/2021JD035476 by University Of Oslo Central 340, Wiley Online Library on [21/10/2022]. See the Terms and Conditions (https://onlinelibrary.wiley.com/terms-and-conditions) on Wiley Online Library for rules of use; OA articles are governed by the applicable Creative Commons License

($E_{TOA-Krakow}$ and e.g., $E_{TOA-China}$). The gridded TOA values are obtained from the Earth system model CESM2, and it is here assumed that this value is well-known and fairly constant across models since it does not depend on Earth's climate. A scaling factor, S, was computed for the Krakow measurement period 2004–2007:

$$S = \frac{109\frac{W}{m^2}}{E_{TOA-Krakow\ (2004-2007)}},$$

and this was multiplied by E_{TOA} in each region for the period 1961–2014, resulting in four scaled average E_{cloudy} values relevant for the study herein:

- United States: 126.7 W/m^2
- China: 134.3 W/m^2
- Japan: 133.6 W/m^2
- Europe: 114.4 W/m^2

These values represent the average SSR during cloudy conditions in each region, based upon measurements from Krakow. The sensitivity of the no-cloud SSR computation to the magnitude of these values is explored in Section 4.2.

4 Results

This section presents results in the following order: In Section 4.1, all-sky SSR from ngGEBA is compared to no-cloud SSR computed from ngGEBA and CRU TS using constant E_{cloudy} values presented in Section 3.2. Next, in Section 4.2, the sensitivity of no-cloud SSR is assessed by varying E_{cloudy}. Section 4.3 compares no-cloud SSR to aerosol emission inventories in each region, and sections 4.4, 4.5, 4.6 and 4.7 investigate these variations in simulated SSR from CMIP6.

4.1 Cloud effects on observed SSR

The goal in this section is to determine to what degree trends in SSR may be caused by trends in cloud cover through cloud-radiation interactions. In this endeavor, the ngGEBA all-sky SSR ($E_{all-sky}$) is compared to the no-cloud SSR ($E_{no-cloud}$), as computed from ngGEBA and CRU TS cloud cover using the method described in Section 3.2 with E_{cloudy} set to the scaled Krakow-values.

Figure 2 shows no-cloud SSR ($E_{no-cloud}$) and all-sky SSR ($E_{all-sky}$), calculated as averages over all ngGEBA stations within the respective regions. The cloud cover data used for each is included in Figure B in Appendix B. No-cloud SSR is higher than all-sky SSR in absolute magnitude, and this is expected since no-cloud SSR contains only SSR values above the cloudy-sky threshold (E_{cloudy}). To facilitate comparison, the range of the vertical axis is identical across all sub-figures of Figure 2, clearly conveying the difference in trend magnitudes between regions.

Figure 2 also shows that no-cloud SSR exhibits stronger trends than all-sky SSR in all regions. In general, across regions, the sign of change in time is the same between no-cloud- and all-sky SSR, but the magnitude of change in time is much stronger in no-cloud SSR. This indicates that cloud cover has a dampening effect on both dimming and brightening trends in observed all-sky SSR. This, in turn, indicates that cloud cover trends are not a contributor to dimming and brightening in the regions studied here.

This article is protected by copyright. All rights reserved.

Accepted Article

21698996, ja, Downloaded from https://agupubs.onlinelibrary.wiley.com/doi/10.1029/2021JD035476 by University Of Oslo Central 340, Wiley Online Library on [21/10/2022]. See the Terms and Conditions (https://onlinelibrary.wiley.com/terms-and-conditions) on Wiley Online Library for rules of use; OA articles are governed by the applicable Creative Commons License

Accepted Article

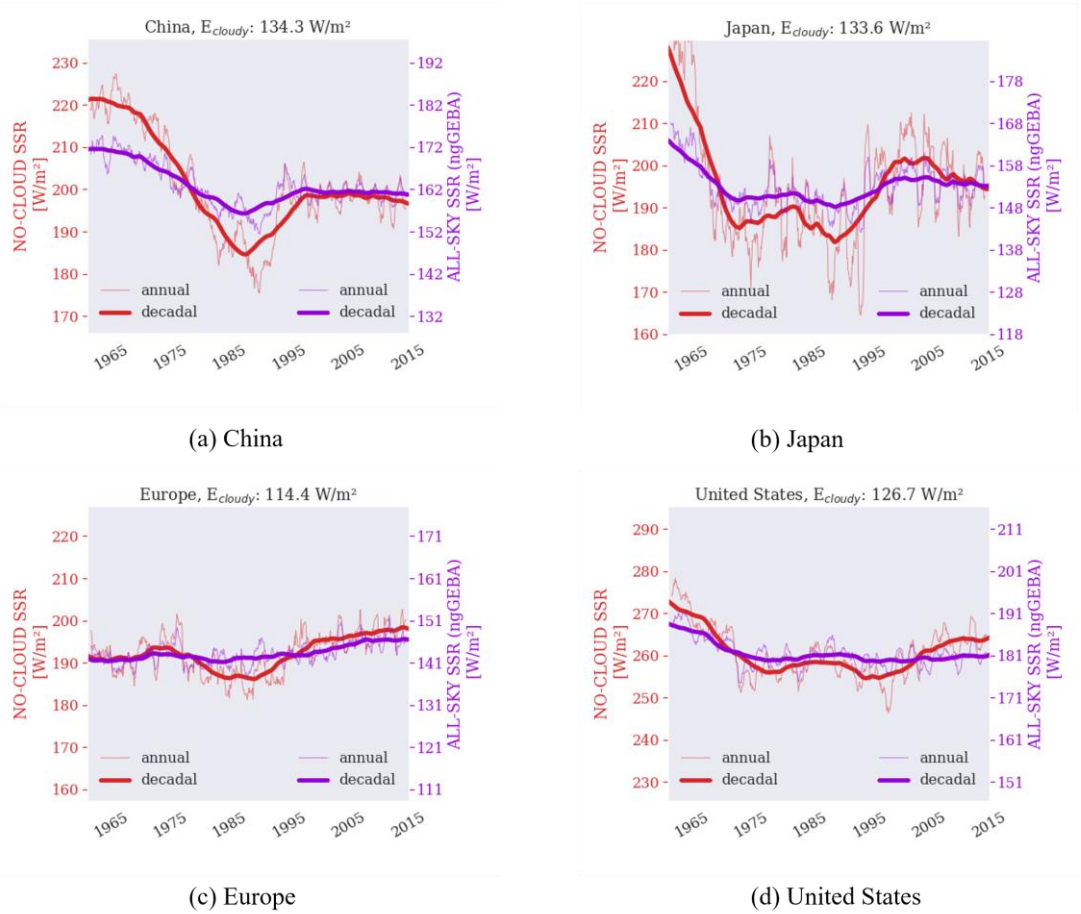

Figure 2: No-cloud SSR (red) and all-sky SSR (purple) between 1961 and 2014 averaged over the ngGEBA stations in the respective regions. Decadal running means are shown in boldface and annual running means are shown in lightface. Vertical scaling is shifted, but equal, between SSR variants and regions. The $\boldsymbol{E_{cloudy}}$ values used for computation of no-cloud SSR (indicated above each sub-figure) are the regionally scaled Krakow-values, discussed in Section 3.2.

It was stated in Section 2.1 that some inhomogeneity issues have been discovered with the ground-based SSR data in China, affecting the trendline change during the 1990s (Figure 2a). The implications of this are further discussed in Section 4.3.1.

Although the trendlines of all-sky and no-cloud SSR are correlated in these regions, some apparent trends are revealed when removing the effects of varying cloud cover. In Japan (Figure 2b), the no-cloud trendline notably exhibits an apparent renewed dimming after 2000, while the all-sky trend only exhibits weak dimming (hardly discernible), suggesting reduced cloud cover strongly counteracts other effects that reduce SSR in that period. In the United States, on the other hand, the no-cloud SSR trendline exhibits a clear brightening trend between the late 1990s and 2014, which is hardly discernible in all-sky SSR, suggesting an increased cloud cover in this period has concealed this no-cloud trend. To the knowledge of the authors, these concealed SSR trends in Japan and the United States have not been identified elsewhere in literature.

4.2 E_{cloudy} and the sensitivity of no-cloud SSR

Earth system models (ESMs) provide output of both all-sky and clear-sky SSR, along with cloud cover. This allows for a computation of E_{cloudy}'s variation in time in simulations; in other words, the SSR during cloudy conditions can be worked out. To do so, clear-sky SSR

This article is protected by copyright. All rights reserved.

21698996, ja, Downloaded from https://agupubs.onlinelibrary.wiley.com/doi/10.1029/2021JD035476 by University Of Oslo Central 340, Wiley Online Library on [21/10/2022]. See the Terms and Conditions (https://onlinelibrary.wiley.com/terms-and-conditions) on Wiley Online Library for rules of use; OA articles are governed by the applicable Creative Commons License

is substituted for $E_{no-cloud}$ in Equation 2 and the equation is solved for E_{cloudy}.

Figure 3 shows E_{cloudy} computed from the CMIP6 multi-model means, collocated to the ngGEBA stations, where each timeseries of cloud cover and SSR is computed into a running annual average before computing E_{cloudy} from the timeseries. The figure reveals how E_{cloudy} varies with time in the simulations and that the spread is larger here than in the scaled Krakow-values. It is also evident that E_{cloudy} is not stationary. In the span of the period 1961–2014, the value has a trend in all the regions; albeit not with the same magnitude or sign. These changes are arguably due to changes in input aerosol/precursor emissions in these regions: Higher emissions may cause lower E_{cloudy} due to a higher number of cloud condensation nuclei and thus smaller cloud droplets. It must be noted that this hypothesis does not directly explain what is happening in Japan, since the Japanese emissions decrease rapidly after 1970; however, the simulated transport of aerosols from the Asian mainland largely affects the Japanese airspace, meaning they may be affecting the Japanese clouds to a significant degree, causing E_{cloudy} to decrease there, too.

Both the regionally scaled Krakow-values and the CMIP6-values may be used as E_{cloudy} in a computation of no-cloud SSR at the ngGEBA stations. Before choosing which to use, it is necessary to assess how sensitive the computation of no-cloud SSR is to the value of E_{cloudy}. To explore this sensitivity, various fixed values for E_{cloudy} were used to compute no-cloud SSR from observed all-sky SSR and cloud cover. The regional running decadal averages (dubbed *trendlines* from now on) of observed all-sky SSR were presented in Figure 2 in Section 4.1; those of cloud cover are presented in Figure B in Appendix B.

The results of the no-cloud SSR computations for various E_{cloudy} are presented in Figure 4, with E_{cloudy} set in five different ways, for each region: a lower value of 90 W/m^2, the Krakow-value of 109 W/m^2, the regionally scaled Krakow-values and that computed from the CMIP6 models for each respective region, both as a variable and as a constant average. It can be gathered from the figure that the general features of the no-cloud SSR timeseries are not strongly influenced by the choice of E_{cloudy}. Magnitudes of change are influenced to some degree, but the locations of maxima and minima are the same across different values for E_{cloudy} with the exception of the European trendline with $E_{cloudy} = 90\ W/m^2$, which exhibits a dimming after 2000.

It is therefore concluded that the general features of the no-cloud SSR trendlines are not sensitive to the choice of E_{cloudy}. In the subsequent sections, an observational study and a CMIP6 study will follow, where the following choices are made: In the observational study, the scaled Krakow-values will be used as E_{cloudy}, based on the fact that these scaled values are ultimately also observed and a mixture of simulated and observed values are avoided. In the CMIP6 study, the multi-model mean values of simulated E_{cloudy} printed in the legend of Figure 3 are utilized.

4.3 Aerosol effects on observed SSR

In this section, the goal is to determine how aerosol/precursor emissions affected observed SSR from 1961 to 2014. To investigate, observed no-cloud SSR (same as studied in Section 4.1) is compared to aerosol/precursor emissions to distinguish what effect aerosols have on no-cloud SSR—without the masking effect from cloud cover variations. Once again, one must keep in mind that the subtraction method used to produce the no-cloud SSR timeseries did not subtract out potential effects of aerosols on *cloud optical properties*. This section compares aerosol/precursor emission trends along with the no-cloud SSR trends for all four regions of focus.

This article is protected by copyright. All rights reserved.

Accepted Article

21698996, ja, Downloaded from https://agupubs.onlinelibrary.wiley.com/doi/10.1029/2021JD035476 by University Of Oslo Central 340, Wiley Online Library on [21/10/2022]. See the Terms and Conditions (https://onlinelibrary.wiley.com/terms-and-conditions) on Wiley Online Library for rules of use; OA articles are governed by the applicable Creative Commons License

Accepted Article

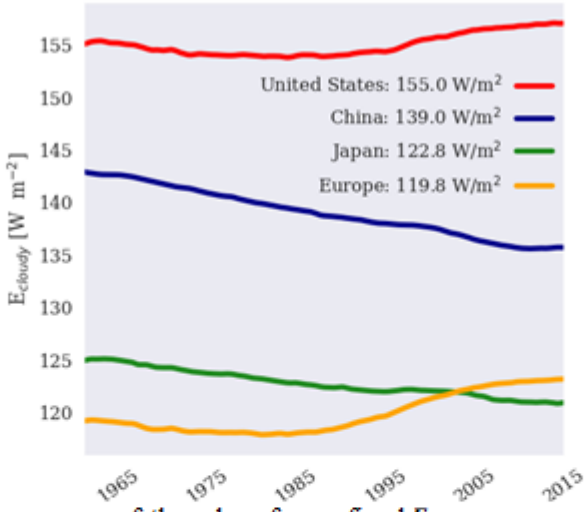

Figure 3: Decadal running average of the value of an unfixed E_{cloudy} as computed from multi-model mean in historical CMIP6 experiments, collocated to the ngGEBA stations in each region. In each legend item, the average of the respective region's E_{cloudy} trendline is printed.

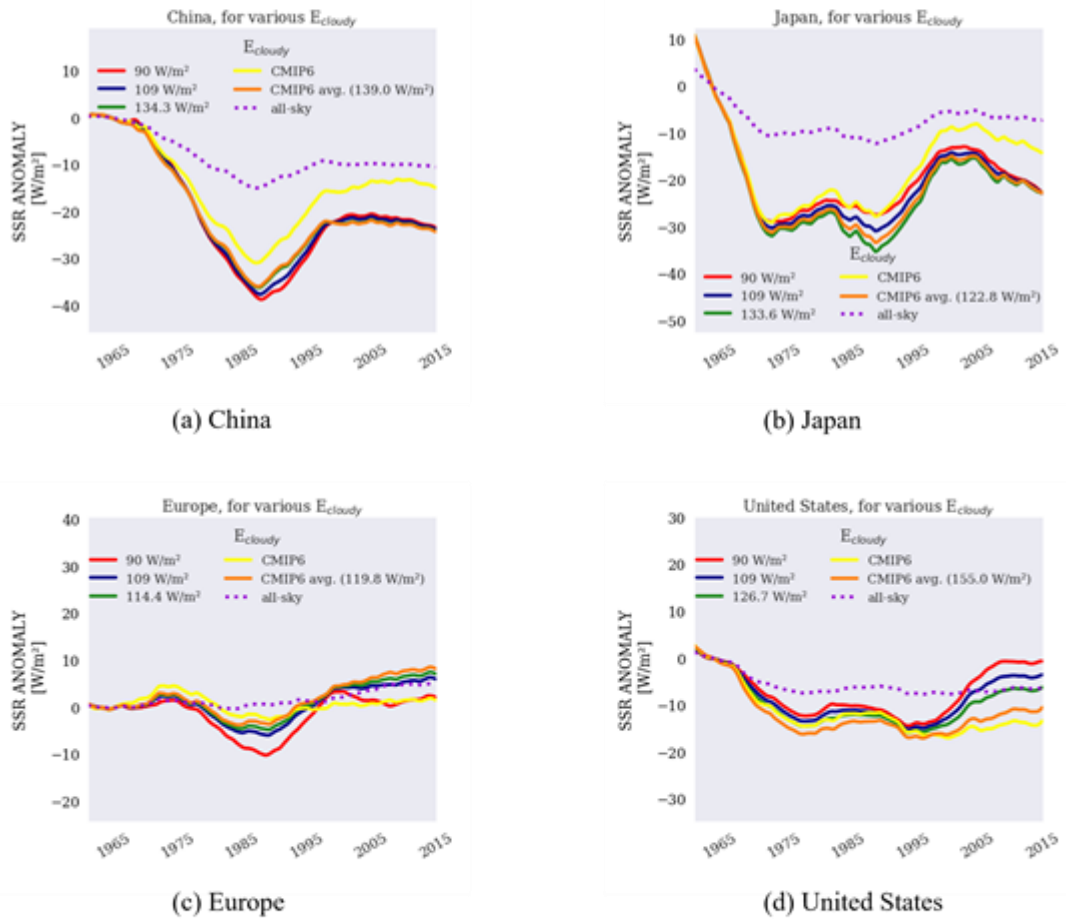

Figure 4: Anomalies of decadal running averages of (solid lines) no-cloud SSR computed using SSR from ngGEBA and cloud cover fraction from CRU TS v4.02 and various values for E_{cloudy} ; (dotted, purple lines) all-sky SSR. Green is computed using regionally scaled values observed in Krakow, Poland; orange and yellow are computed using values computed from CMIP6 multi-model means (see Figure 2); in yellow, the unfixed values shown in Figure 2, in orange, the average value constant. All data is collocated to the ngGEBA stations in each region. The anomalies are computed by averaging the initial 5 years of the running mean time series, and subtracting this mean value from each time step.

This article is protected by copyright. All rights reserved.

21698996, ja, Downloaded from https://agupubs.onlinelibrary.wiley.com/doi/10.1029/2021JD035476 by University Of Oslo Central 340, Wiley Online Library on [21/10/2022]. See the Terms and Conditions (https://onlinelibrary.wiley.com/terms-and-conditions) on Wiley Online Library for rules of use; OA articles are governed by the applicable Creative Commons License

Accepted Article

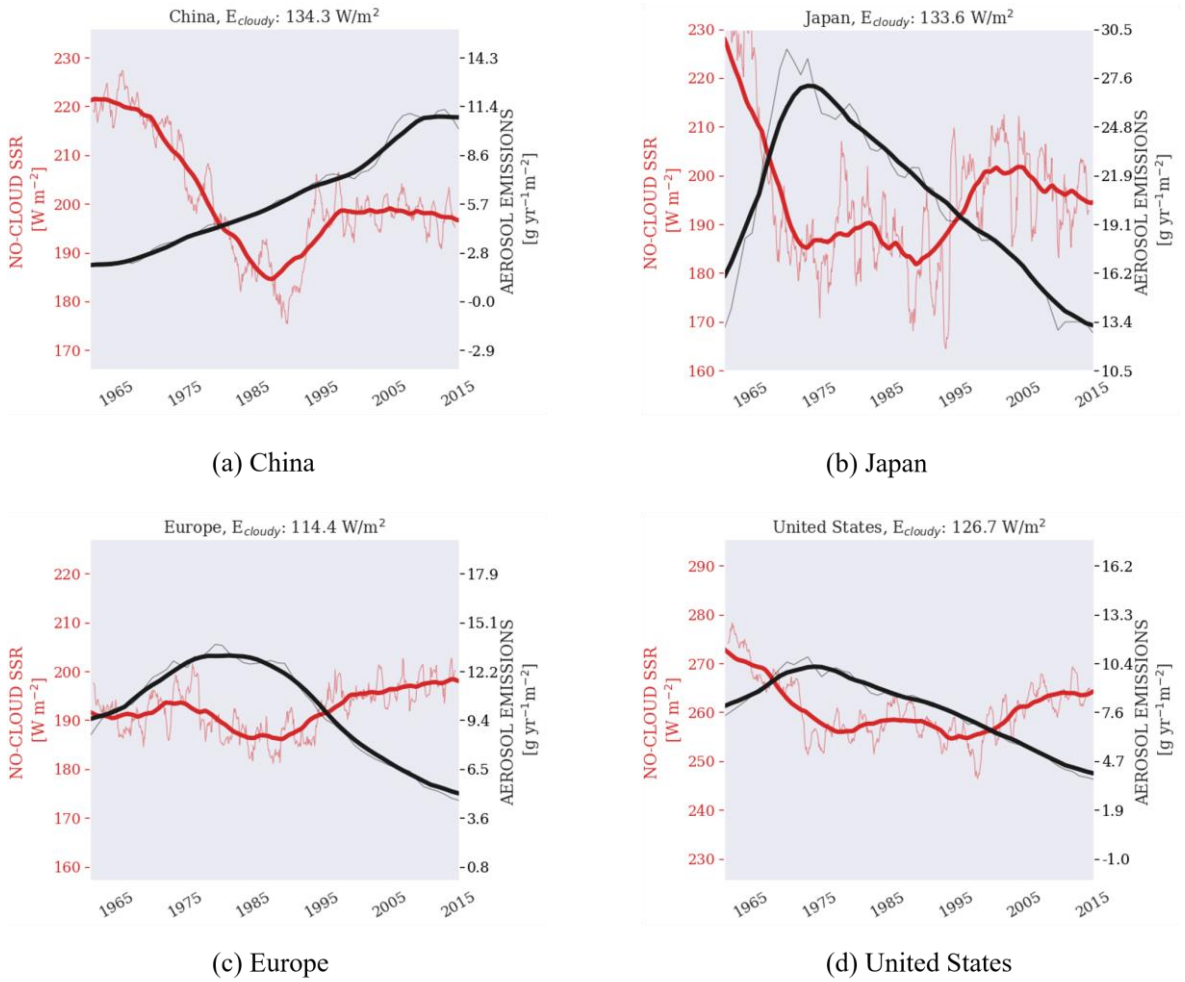

Figure 5: Trendline comparison of no-cloud SSR from ngGEBA and aerosol/precursor emissions from 2020 CEDS (sum of SO_2, NH_3, black carbon, organic carbon, NO_X and NMVOC). Decadal running means in boldface and annual running means in lightface. Assumed constant cloud SSR: 109 W/m².

Figure 5 shows total emissions of aerosols and aerosol precursors from each region, normalized using each region area (as described in Section 3.1), and no-cloud SSR. It can be immediately gathered that the initial dimming seen in China, Japan, Europe and the United States happens simultaneous to general increase in aerosol/precursor emissions. This suggests that aerosol effects caused the initial decrease in no-cloud SSR in these regions.

Soon after the initial dimming, China, Japan and the United States no longer exhibit a clear anticorrelation with the emission trends. This indicates that the sum total aerosol/precursor emissions are not obviously the main cause of subsequent brightening or stabilization in no-cloud SSR.

It should be noted that Japan is a small region, and it is necessarily strongly influenced by other regions' aerosol/precursor emission trends, especially due to its position downwind from the Asian mainland (because of the prevailing westerly winds). China is upwind from Japan, and Chinese emissions exhibit a trendline quite different from that of Japanese emissions. It can be hypothesized that the no-cloud SSR trendline over Japan is increasingly affected by increased emissions elsewhere, for instance Chinese or Indian emissions. Hypothetically, an aerosol/precursor emission trendline including emissions from Japan and countries upwind from Japan may exhibit a trend more anticorrelated with no-cloud SSR than that of only Japanese emissions shown in Figure 4b, but this analysis is

This article is protected by copyright. All rights reserved.

21698996, ja, Downloaded from https://agupubs.onlinelibrary.wiley.com/doi/10.1029/2021JD035476 by University Of Oslo Central 340, Wiley Online Library on [21/10/2022]. See the Terms and Conditions (https://onlinelibrary.wiley.com/terms-and-conditions) on Wiley Online Library for rules of use; OA articles are governed by the applicable Creative Commons License

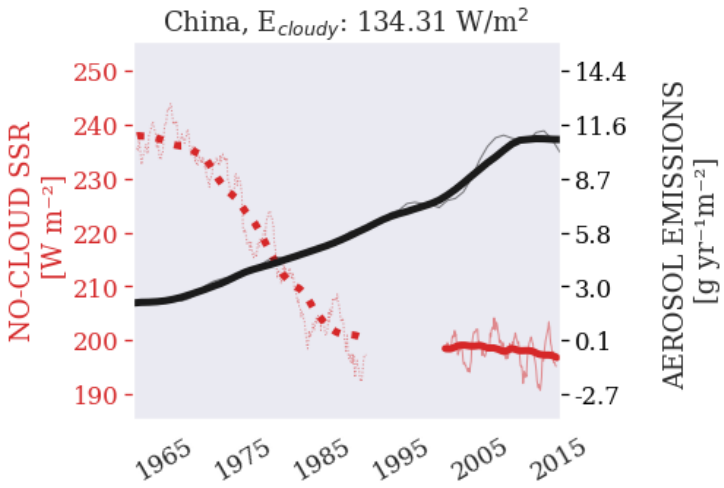

Figure 6: Altered version of Figure 4a, assuming that the ngGEBA brightening trend during the 1990s is an artifact of instrumentation (Wang and Wild, 2016). This figure is comparable to Figure 10 in Yang, et al. (2018), wherein 7 W/m^2 is the approximate difference between the 1990 averages of unhomogenized and homogenized SSR. In this figure, the dotted, red line is the "homogenized" version of decadal no-cloud SSR trend, computed from the original ngGEBA all-sky SSR trend raised +7 W/m² between 1961 and 1990 and CRU TS cloud cover, with $\boldsymbol{E_{cloudy}}$ set to the Krakow-value scaled to China (134.3 W/m^2). The solid, red line is the same no-cloud ngGEBA as in 4a between 2000 and 2014. The boldface black line is the decadal trend in annual aerosol/precursor emissions (sum of SO_2, NH_3, black carbon, organic carbon, NO_X and NMVOC) from 2020 CEDS in China, the lightface is the annual data. Assumed constant cloud SSR: 109 W/m².

beyond the scope of this study.

In Europe (Figure 5c), the maximum in emissions is reached around 1980, approximately concurrent with the minimum in no-cloud SSR, which indicates that emissions of aerosols are contributing to the SSR dimming and subsequent brightening. However, Figure 5c also reveals a brightening in no-cloud SSR during the 1970s which cannot be explained by the aerosol/precursor emissions trendline.

4.3.1 Altered no-cloud SSR in China

As explained in Section 2.1, the Chinese brightening trend during the 1990s has been argued to be an artifact of instrumentation change. To visualize and investigate the effects of a homogenization of ngGEBA, a crude attempt has been made to homogenize the trendline along the lines of Yang, et al. (2018). Figure 6 shows the resulting no-cloud SSR, and the figure caption contains a description of how the "homogenized" trendline is computed from ngGEBA. Assuming the altered trendline to be correct, the aerosol/precursor emissions seem able to explain the entire SSR trend until around 2010, when the aerosol/precursor emissions begin decreasing. It should be noted that the rigorously computed timeline in Yang, et al. (2018) exhibits a brightening after 2010, which is not reproduced in Figure 6; a brightening better matches the emissions trendline, which exhibits the beginnings of a reversal around the same time. Such a brightening is also present between 2010 and 2016 in another previous work, where a clear-sky SSR trend is computed from daily data in China (Yang, et al., 2019) (Yang, et al., 2019). The reason for the absence of the reversal in the no-cloud SSR trendline is unclear, but is difficult to investigate due to the brevity of the period in question, 2010-2014. Furthermore, as mentioned in Section 2.3, according to Wang, et al. (2021), a different version of anthropogenic aerosol emissions of China exhibited a decreasing trend after 2005, which is also in better agreement with a brightening.

This article is protected by copyright. All rights reserved.

Accepted Article

21698996, ja, Downloaded from https://agupubs.onlinelibrary.wiley.com/doi/10.1029/2021JD035476 by University Of Oslo Central 340, Wiley Online Library on [21/10/2022]. See the Terms and Conditions (https://onlinelibrary.wiley.com/terms-and-conditions) on Wiley Online Library for rules of use; OA articles are governed by the applicable Creative Commons License

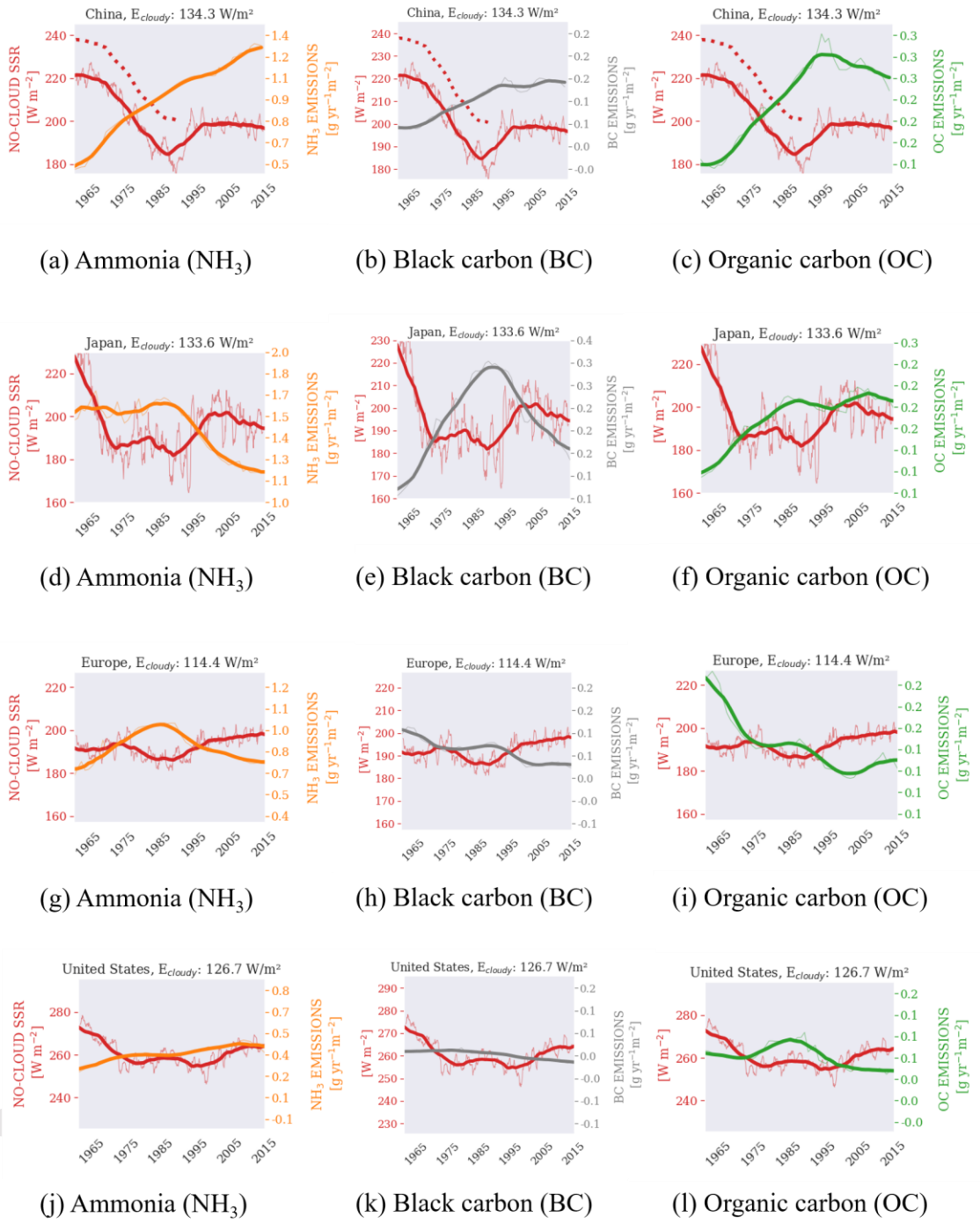

Figure 7: No-cloud SSR trendlines from ngGEBA shown in red, annual emissions of individual species from 2020 CEDS are shown in orange (NH_3), grey (BC) and green (OC). Decadal running average in boldface and annual running average in lightface. Assumed constant cloud SSR is different for each region, printed above each sub-figure. Each row contains data from one region, from top to bottom: China, Japan, Europe and the United States. The dotted line in the sub-figures on the top row is the "homogenized" no-cloud SSR shown in Figure 6.

It should be noted that there is a sudden increase also in Japanese no-cloud SSR during the 1990s. This similarity was also pointed out by Moseid, et al. (2020). No significant instrumentation changes have been documented in Japan and the no-cloud SSR trendline cannot be explained by the total aerosol emissions, but in Section 4.3.2 a possible contributing cause is discussed.

This article is protected by copyright. All rights reserved.

Accepted Article

21698996, ja, Downloaded from https://agupubs.onlinelibrary.wiley.com/doi/10.1029/2021JD035476 by University Of Oslo Central 340, Wiley Online Library on [21/10/2022]. See the Terms and Conditions (https://onlinelibrary.wiley.com/terms-and-conditions) on Wiley Online Library for rules of use; OA articles are governed by the applicable Creative Commons License

Accepted Article

21698996, ja, Downloaded from https://agupubs.onlinelibrary.wiley.com/doi/10.1029/2021JD035476 by University Of Oslo Central 340, Wiley Online Library on [21/10/2022]. See the Terms and Conditions (https://onlinelibrary.wiley.com/terms-and-conditions) on Wiley Online Library for rules of use; OA articles are governed by the applicable Creative Commons License

4.3.2 Individual aerosol species effects on observed SSR

The trendlines of total aerosol/precursor emissions in Figure 4 are unable to explain the entirety of the observed trends in SSR, calling upon a continued investigation into potential causes.

The total emissions of aerosols/precursors from China, Japan, Europe and the United States are dominated by SO_2 (precursor), NOx (precursor) and NMVOC (precursor). The emission trendlines of these dominating species all show variation similar to the total aerosol/precursor emissions between 1961 and 2014. In the following, the relatively minor contributors to the total aerosol/precursor emissions are compared to the no-cloud SSR trends in order to shed some light on the trends of the minor emissions that do not necessarily correlate with the total emission trend. These relatively minor emissions are those of NH_3 (precursor), black carbon (aerosol) and organic carbon (aerosol).

It should be realized that if these relatively small contributors can explain the SSR effects observed, their individual contributions to extinction of solar radiation must necessarily be much larger per mass emitted than their dominating counterparts. This may especially be the case for organic and black carbon because they are aerosols upon emission (as opposed to precursor gases), and start to scatter and absorb solar radiation upon emission; precursor gases (SO_2, NO_x, NMVOC and NH_3) may be advected out of the region of interest before reacting into particulate matter. In addition, extinction properties vary between species of aerosols; black and brown carbon aerosols both scatter and absorb, while sulfuric aerosols only scatter radiation. In fact, recent evidence suggests that changes in atmospheric shortwave absorption contribute significantly to SSR trends in both China and Europe (Schwarz, et al., 2020). For these reasons, it can be assumed that black and organic carbon emissions have a larger contribution to extinction per mass emitted than the other species. That said, it is not completely straightforward to estimate the differences quantitatively when studying aerosol emissions.

Figure 7 compares the trendlines of no-cloud SSR—for each region—with the individual emissions of ammonia, black carbon and organic carbon, which are minor parts of the total aerosol/precursor emissions in all the regions. It is noticeable that the emission maxima/minima occur at different times compared to those in the total aerosol/precursor emissions (as seen in Figure 5).

Figure 7a–c shows emissions of NH_3, black carbon and organic carbon compared to no-cloud SSR in China. These sub-figures contain both the unaltered no-cloud SSR (solid red line) and the "homogenized" no-cloud SSR (dotted red line pre-1990). The individual species emissions all increase for the entirety of the dimming period, similar to the sum total emissions (Figure 5a and 6). The figure reveals that emissions of organic carbon reverse during the late 1990s, but this reversal occurs after the switch to brightening in unaltered no-cloud SSR (solid red trendline). None of the emissions anticorrelate with the unaltered no-cloud SSR during the reversal of the 1990s. Like the sum total emissions, the trendlines of NH_3 and black carbon are anticorrelated with the "homogenized" no-cloud SSR for most of the period 1961–2014. The levelling off in "homogenized" no-cloud SSR after the 1990s may possibly be explained by a slowdown of black carbon emission increase combined with a reduction in organic carbon emissions.

In Japan (Figure 7d–f), the trendlines of NH_3, black carbon and organic carbon are all to some degree anticorrelated with the SSR trendline between 1980 and 2000. The emissions reach a maximum almost simultaneous to the intermittent minimum around 1990 in the no-cloud SSR brightening, which could point to decreased emission of these species contributing to the 1990s brightening as mentioned previously. That said, the renewed dimming in no-cloud SSR after 2000 is not consistent with any of the emission trendlines. And as previously

This article is protected by copyright. All rights reserved.

Accepted Article

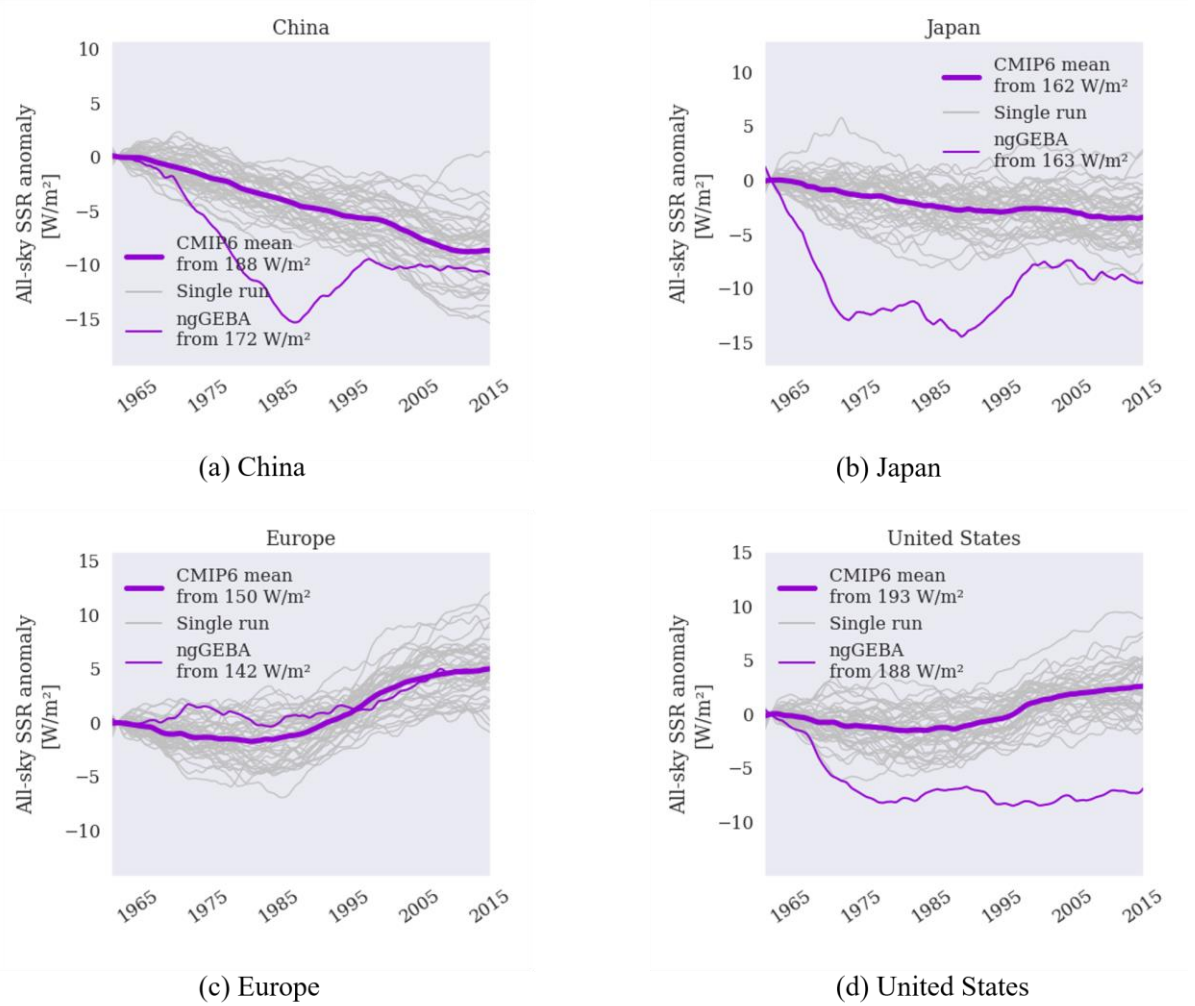

Figure 8: Decadal running means of mean simulated (CMIP6) and observed (ngGEBA) all-sky SSR anomalies between 1961 and 2014 averaged over ngGEBA stations in four regions: Multi-model mean CMIP6 in boldface and ngGEBA in lightface. Grey lines are decadal running means of each model run included. The anomalies are computed by averaging the initial 5 years of the running mean timeseries (this average is printed after "from" in the legend items), and subtracting this mean value from each subsequent time step. Included in the computation is a CMIP6 historical all-forcing simulation (r1i1f1p1) from each of the 42 models presented in Table 1.

noted, the atmosphere in the Japanese region is largely affected by emissions from mainland Asia, including Chinese emissions.

In Europe (Figure 7g–i), the emissions of black and organic carbon exhibit interesting trendlines in relation to the no-cloud SSR variations, as the trendlines of these emissions somewhat anticorrelate with the no-cloud SSR trendline. Especially notable, the local maximum in no-cloud SSR during the 1970s happens simultaneous to local minima in black and organic carbon, and that could possibly be an explanation for this intermittent brightening during the dimming phase in Europe.

Figure 5d showed that in the United States, no-cloud SSR anticorrelates with the total aerosol/precursor emissions until the late 1980s, at which point no-cloud SSR begins exhibiting a renewed dimming concurrent with a continued decrease in emissions. Figure 7 (j–l) shows that NH_3 emissions generally increase throughout the period in question, but none of the species shows an increase starting in the late 1980s. Thus, the intermittent dimming in

This article is protected by copyright. All rights reserved.

21698996, ja, Downloaded from https://agupubs.onlinelibrary.wiley.com/doi/10.1029/2021JD035476 by University Of Oslo Central 340, Wiley Online Library on [21/10/2022]. See the Terms and Conditions (https://onlinelibrary.wiley.com/terms-and-conditions) on Wiley Online Library for rules of use; OA articles are governed by the applicable Creative Commons License

no-cloud SSR in the United States from the late 1980s until the mid-1990s cannot clearly be attributed to aerosol emission changes.

4.4 Bias in simulated SSR

As introduced previously, ESMs have been found not to be able to reproduce the full extent of the dimming in SSR. To the knowledge of the authors, only a small subset of the latest generation of ESMs (CMIP6) has been studied with regards to dimming and brightening (Moseid et al., 2020). This section investigates the average of 42 historical all-forcing simulations of all-sky SSR from 42 models participating in CMIP6 (listed in Table A of Appendix A), in comparison to the observed all-sky SSR trends seen in ngGEBA.

Figure 8 shows the anomalies of all-sky SSR in the CMIP6 simulation mean compared to ngGEBA, and reveals that the ESMs remain unable to reproduce the magnitude of dimming observed at ngGEBA sites in China, Japan and the United States. This was found for many regions in the previous generation of ESMs as well (Allen, et al., 2013; Storelvmo, et al., 2018; Wild & Schmucki, 2010), and confirms for a larger set of CMIP6 models the same conclusion made for a subset of these models by Moseid et al. (2020).

The brightening trend in Europe after the 1980s is fairly well reproduced in CMIP6, as found for the model subset of 8 ESMs studied in Moseid et al. (2020). If it is assumed that the emission inventory of Europe accurately represents reality, this suggests that the models are, indeed, able to translate emissions into optical depth and SSR. However, this might indicate that the emission inventories of the other regions studied here (China, Japan and the United States) are erroneous. Otherwise, as suggested in Storelvmo et al. (2018) for a previous generation of ESMs, the models may be unable to translate emissions into optical depth and SSR correctly, despite their ability to translate them fairly accurately into SSR changes in Europe.

In China (Figure 8a), even if the trend in the 1990s is a result of artifacts (see Section 2.1), the CMIP6 simulations are highly biased, showing a dimming of around 5 W/m^2 in 1961–1980 when ngGEBA shows a dimming of more than 15 W/m^2.

Having studied the all-sky trends, the following sections investigate potential causes for these biases and differences by looking instead at clear-sky and no-cloud SSR, which removes the changes in SSR due to clouds and cloud cover changes.

4.5 Aerosol effects on simulated SSR

In this section, an investigation is made into what effects aerosol/precursor emissions have on the dimming and brightening that is present in the simulations, regardless of how these compare to observations. It should be noted that the aerosol/precursor emissions shown here are not exactly the same as those studied in the observational analysis in Section 4.3, because the CMIP6 simulations are forced by an older version of CEDS. Differences between the datasets that are relevant for this paper are decreases in Chinese emissions of certain aerosol species after 2000 (see Section 2.3). The purpose of this section is to study the relationship between input emissions and simulated SSR, as presented in Figure 9, which also shows the differences between all-sky, clear-sky and no-cloud SSR, where no-cloud SSR is computed using the average E_{cloudy} from the CMIP6 models as presented in Section 4.2. The differences between the different variants of SSR are discussed in Section 4.6.

It was found in Section 4.4 that the simulated SSR trend in the CMIP6 simulations exhibits a too-weak dimming in China. Nonetheless, a relatively slight dimming was evident. Now, the question is whether aerosol/precursor emissions caused the slight dimming in the simulations. Figure 9a shows a comparison between simulated all-sky, no-cloud and clear-sky SSR and input aerosol/precursor emissions. It is evident from the figure that the SSR

This article is protected by copyright. All rights reserved.

Accepted Article

21698996, ja, Downloaded from https://agupubs.onlinelibrary.wiley.com/doi/10.1029/2021JD035476 by University Of Oslo Central 340, Wiley Online Library on [21/10/2022]. See the Terms and Conditions (https://onlinelibrary.wiley.com/terms-and-conditions) on Wiley Online Library for rules of use; OA articles are governed by the applicable Creative Commons License

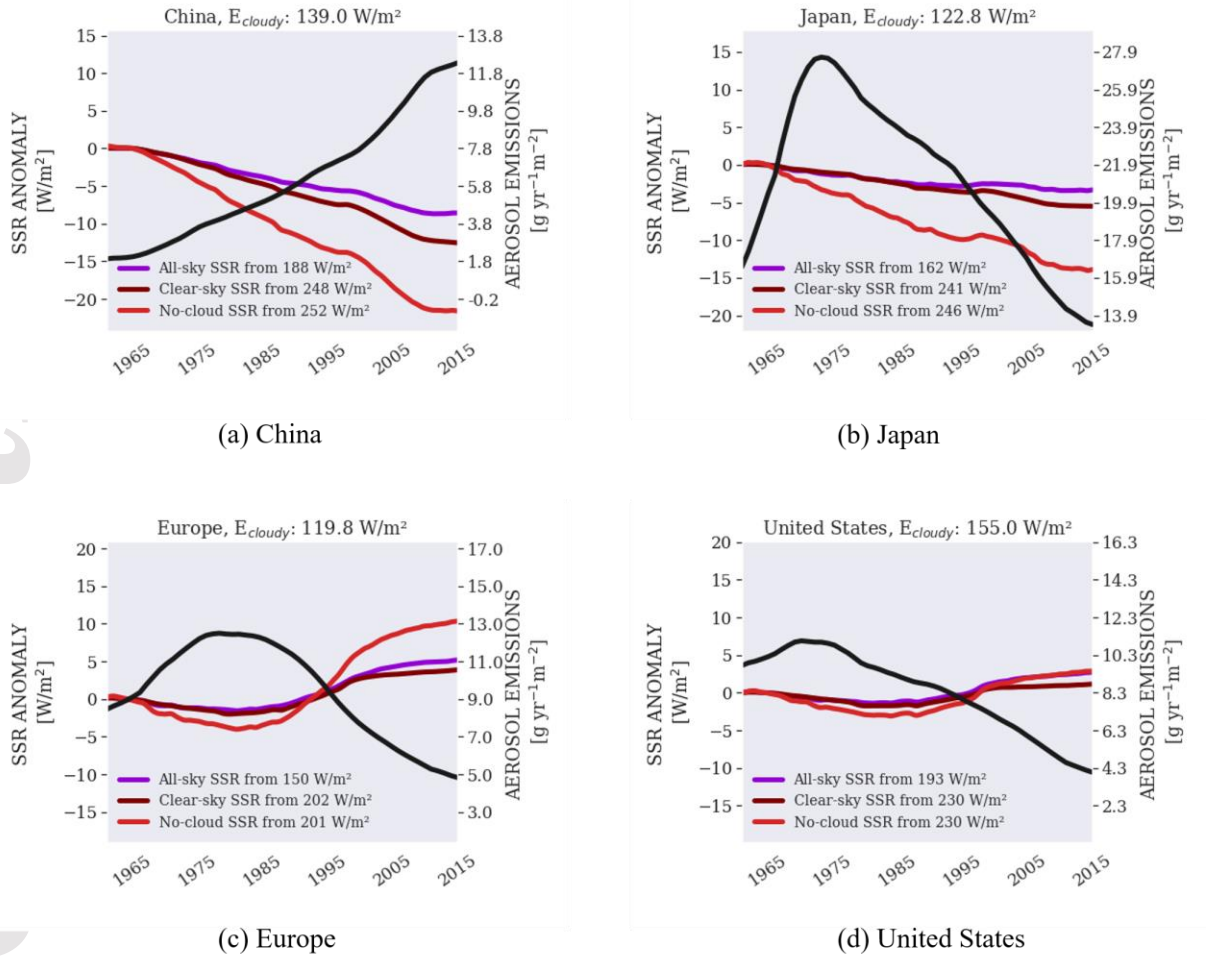

Figure 9: Decadal running means of mean simulated (CMIP6) all-sky-, clear-sky- and no-cloud SSR anomalies and input aerosol/precursor emissions (sum of SO_2, NH_3, black carbon, organic carbon, NO_X and NMVOC between 1961 and 2014 at ngGEBA station locations: all-sky SSR in purple; clear-sky SSR in maroon; no-cloud SSR in bright red; aerosol/precursor emissions in black. The $\boldsymbol{E_{cloudy}}$ utilized for the no-cloud SSR computation are computed from the CMIP6 models, previously shown in Figure 2. Included in the no-cloud SSR mean is one CMIP6 simulation (r1i1f1p1) from each of the 42 models presented in Table A in Appendix A.

trend (all variants) mirrors the aerosol/precursor emission trend, suggesting a strong dependence, at least qualitatively. Throughout the period 1961–2014, the trendlines are almost perfectly anticorrelated. In the observational study (Section 4.3), an anticorrelation was also found between no-cloud SSR and aerosol/precursor emissions, assuming that the altered trendline (Figure 6) is correct. If the altered trendline represents reality, the bias between observed and simulated SSR may be caused by a model issue with the translation of emissions into realistically high optical depths, or that the magnitude of the input emissions is simply too low.

Section 4.4 showed that also in Japan, the simulated dimming was weaker than observed. In addition to the too-weak magnitude of dimming, the simulated SSR trend is continuously negative throughout the period 1961–2014, which is not seen in observations. The question herein is what effect the input aerosol/precursor emissions have on the simulated SSR, and Figure 9b reveals that there is no clear relationship between the trendlines of SSR and aerosol/precursor emissions. Recalling that aerosol transport from mainland Asia affects the SSR trend in Japan to a large degree, it is relevant also to compare the Japanese SSR trends to the Chinese input aerosol/precursor emission trend, which is

This article is protected by copyright. All rights reserved.

Accepted Article

21698996, ja, Downloaded from https://agupubs.onlinelibrary.wiley.com/doi/10.1029/2021JD035476 by University Of Oslo Central 340, Wiley Online Library on [21/10/2022]. See the Terms and Conditions (https://onlinelibrary.wiley.com/terms-and-conditions) on Wiley Online Library for rules of use; OA articles are governed by the applicable Creative Commons License

continuously increasing in the study period (Figure 9a). Clearly, the Japanese SSR trends are better anticorrelated with the Chinese emissions. However, the SSR trend is still too weak, which could be a result of one or several of the following possibilities, 1) a model issue with translating emissions into realistically high optical depths, 2) too-low input emissions in Japan or mainland Asia, or 3) erroneous simulated aerosol transport to the Japanese airspace.

For Europe (Figure 9c), the previous section concluded that the all-sky SSR trend is well reproduced by the models. Figure 9c reveals that simulated no-cloud SSR and aerosol/precursor emissions are almost perfectly anticorrelated, suggesting a causal relationship in the simulations.

In the United States (Figure 9d), the trendlines of all-sky SSR and that of aerosol/precursor emissions mirror each other quite closely. Knowing that the simulations do not reproduce the magnitude of observed dimming, the same issues as proposed for the Japan simulations are possible, including potential issues linked to transported emissions: Knowing that there is transport of aerosols from Asia to North America (via the prevailing westerly winds), too-low input emissions from mainland Asia could be a contributing cause for a too-weak dimming seen in the United States.

4.6 Differences between all-sky, clear-sky and no-cloud SSR

As mentioned, there are interesting differences between the three SSR variants in Figure 9. Increases in clear-sky SSR are weaker than those in all-sky SSR, and decreases in clear-sky are stronger than all-sky, and this is because cloud cover decreases throughout the study period in all regions (see Figure B in Appendix B); with reduced cloud cover, all-sky SSR increases, but clear-sky SSR is not affected by the cloud change. Thus, with a general increase in SSR, clear-sky SSR increases less than all-sky, and with a general decrease in SSR, clear-sky SSR decreases more than all-sky SSR.

No-cloud SSR is arguably not affected by reduced cloud cover, but it *is* affected by changes in the time-varying cloud SSR (E_{cloudy}). No-cloud SSR, in fact, reacts more strongly to changes in the time-varying E_{cloudy} than does all-sky SSR. As time-varying E_{cloudy} increases beyond the constant E_{cloudy}, the SSR during cloudy conditions contributes more and more to the general increase in SSR. Thus, most clearly in Europe—even though cloud cover is decreasing throughout the period of study—no-cloud SSR exhibits a brightening stronger than that found in both all-sky SSR and clear-sky SSR due to the increase in unfixed E_{cloudy}, as shown in Figure 2.

4.7 Apparent Effect of aerosols on observed and simulated SSR

The purpose of this section is to get a sense of the *apparent* effect of emitted aerosols/precursors on SSR, in both observations and simulations. To estimate a value, the following computation of Apparent Effect is made:

$$Apparent\ Effect = \frac{\Delta E_{no-cloud}}{\Delta Emissions},$$

where $\Delta E_{no-cloud}$ is the change in no-cloud SSR over a certain period and $\Delta Emissions$ is the change in aerosol/precursor emissions over the same period. This value quantifies how no-cloud SSR changes simultaneous to a certain change in emissions, presumably due to direct and indirect aerosol effects on incoming radiation. The Apparent Effect allows for comparison and quantification of the difference between regions and periods and between observations and simulations. The table in Figure 10 shows the result of these computations, made for periods of time when the general trend in no-cloud SSR may be argued to have been

This article is protected by copyright. All rights reserved.

Accepted Article

21698996, ja, Downloaded from https://agupubs.onlinelibrary.wiley.com/doi/10.1029/2021JD035476 by University Of Oslo Central 340, Wiley Online Library on [21/10/2022]. See the Terms and Conditions (https://onlinelibrary.wiley.com/terms-and-conditions) on Wiley Online Library for rules of use; OA articles are governed by the applicable Creative Commons License

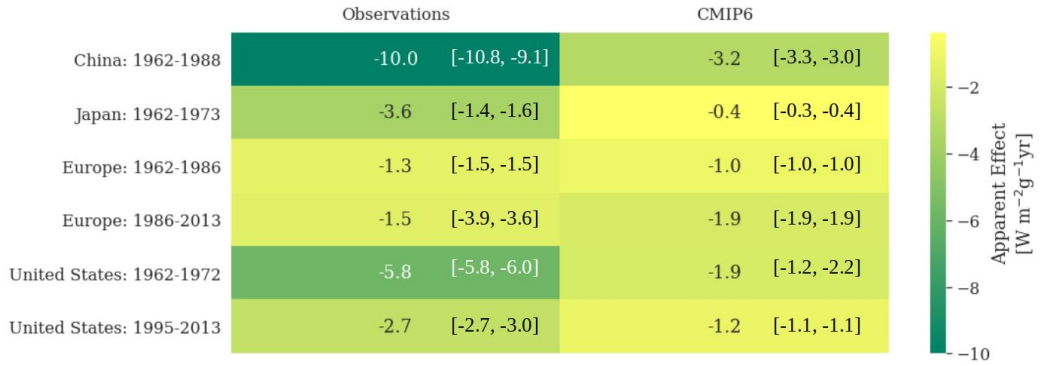

Figure 10: Apparent Effects of emissions of aerosols and precursors ($\Delta\boldsymbol{Emissions}$) on no-cloud SSR ($\Delta\ \boldsymbol{E_{no-cloud}}$), computed from ngGEBA observations, CRU TS v4.02 cloud cover and CMIP6 SSR and cloud cover, and the 2020 CEDS and CMIP6 CEDS aerosol/precursor emissions. The apparent effects are computed from decadal running means. In brackets: The Apparent Effects computed for a temporal window -1 year and +1 year from the range given in the figure, to indicate the uncertainty of the computation. Regions are China, Japan, Europe and the United States (U.S.), and periods are chosen based on constancy in observed trend of no-cloud SSR and emissions. The procedure to compute no-cloud SSR is described in Section 3.2, and the constants used for $\boldsymbol{E_{cloudy}}$ are a) for observations, the regionally scaled Krakow-values and b) for CMIP6, the multi-model mean $\boldsymbol{E_{cloudy}}$ averages, as printed in the legend items of Figure 4.

caused by a trend in aerosol/precursor emissions. In other words, during the periods chosen, trendlines of no-cloud SSR and emissions are anticorrelated; see Figure 5 for the observed no-cloud SSR trendlines and Figure 9 for the CMIP6 simulated no-cloud SSR trendlines. In Europe and the United States, two separate periods are included. Looking first at observations (first column in Figure 10), it is clear that China has an Apparent Effect stronger than any other region by a factor of 1.7-7.7, based on observations. Europe's observed Apparent Effect is the lowest. These variations between regions could have been due to the different general levels of aerosols in the periods chosen, since the radiative effect of increased aerosol load on SSR is stronger in regions of low baseline aerosol load (Swinehart, 1962). In China, the emissions of aerosols started quite low in 1961, as opposed to the other three regions, and this could serve as an explanation for the relatively higher effect upon SSR in China during the initial period. However, Figure 10 also shows that the opposite is true in the United States. There, the effect of aerosol/precursor emissions on SSR is higher between 1961 and 1971 than it is between 1996 and 2014—even though the United States reached its peak emissions during the 1970s, and the mean emissions were lower during the period 1996–2014. It is possible that the change in emissions is not large enough in the United States between the periods 1961–1971 and 1996–2014 for this effect to be noticeable here, and variations in natural aerosols such as dust are also potentially relevant.

Proceeding to study the simulated Apparent Effects, it must be realized that comparisons between observed and simulated quantifications in this regard assumes that the estimated input emissions are accurate; if the emission changes are too small (large), the true Apparent Effect is much weaker (stronger) than that found in the computed observed Apparent Effect, and in this scenario this quantification cannot correctly indicate bias in models.

Nonetheless the quantifications in Figure 10 suggest the following: Compared to observations, the CMIP6 models reproduce the Apparent Effect of aerosol/precursor emissions on SSR fairly well in Europe, but not in other regions. Furthermore, the simulated Apparent Effects in all four regions are fairly close in magnitude to the observed Apparent Effect in Europe. This suggests that despite observed regional differences in the effect of

This article is protected by copyright. All rights reserved.

Accepted Article

21698996, ja, Downloaded from https://agupubs.onlinelibrary.wiley.com/doi/10.1029/2021JD035476 by University Of Oslo Central 340, Wiley Online Library on [21/10/2022]. See the Terms and Conditions (https://onlinelibrary.wiley.com/terms-and-conditions) on Wiley Online Library for rules of use; OA articles are governed by the applicable Creative Commons License

aerosol/precursor emissions on SSR (due to e.g. variations in composition of aerosol load), the CMIP6 models respond to aerosol/precursor emissions in a similar manner in all regions.

As previously noted, the comparison between observed Apparent Effect and simulated Apparent Effect is based on the assumption that the input aerosol/precursor emissions are correct representations of reality. Moseid et al. (2020) proposes that this may not necessarily be true for China, suggesting that emissions are the dominating source of error in simulations of SSR in China.

In this study, it is somewhat difficult to conclude that emissions are the most probable reason why the CMIP6 models fail to simulate correct dimming and brightening in China, Japan *and* the United States; this is because one must then argue that erroneous input emissions cause too-weak dimming in all three regions—one of which is located far away from the others. However, the radiative transmissivity of all three regions are to some extent affected by emissions from mainland Asia, since pollutants travel across the Pacific with the prevailing Westerlies (Zhao, et al., 2006; Lewinschal, et al., 2019). It could therefore potentially be argued that only a single Asian region's emission estimates must be underestimated in CEDS for the Apparent Effect quantity to be affected substantially in all these regions. However, to conclude as such, further work is required in quantifying the necessary magnitude of underestimation in CEDS. And unless a sufficient underestimation can be accounted for, it seems like model issues are contributing to the problem of simulating dimming and brightening correctly.

5 Concluding remarks

This has been an investigation into dimming and brightening trends between 1961 and 2014 in the regions China, Japan, Europe and the United States. Measurements and Earth system model (ESM) simulations have been studied.

The observational study concludes that, in general, observed dimming and brightening have been weakened by cloud cover variations. Certain SSR trends were found to have been completely masked by cloud cover changes in Japan and the United States. Aerosol/precursor emissions appear to have caused the dimming early in the study period in China, Japan, Europe and the United States. The brightening trends following the initial dimming in Japan, Europe and the United States were not found to be directly connected to total aerosol/precursor emissions; however, composition changes in the aerosol/precursor emissions may to a degree be able to explain the brightening in some of these regions.

In China, the brightening trend in the 1990s seen in ngGEBA cannot be explained by the aerosol/precursor emission trend; however, recent literature suggests that the Chinese SSR data contains inhomogeneities due to a transition to new instrumentation. An attempt to crudely correct for this transition indicates that the no-cloud SSR trends can mostly be attributed to the aerosol/precursor emission trend.

It was found that 42 ESMs participating in CMIP6 remain unable to reproduce the magnitude of observed trends in all-sky SSR in China, Japan and the United States, but that they are able to closely simulate observed dimming and brightening in Europe. Simulated cloud cover was found to weaken simulated dimming trends due to general decrease in simulated cloud cover throughout the period in question; input aerosol/precursor emissions were found to mirror the trends in simulated clear-sky SSR in China, Europe and the United States, suggesting causality in the simulations. In Japan, the simulated no-cloud SSR was found to exhibit an anticorrelation with input aerosol/precursor emissions from China, indicating a clear influence in simulated Japanese SSR.

The Apparent Effects (see Section 4.6) of input aerosol/precursor emissions on SSR in simulations across regions were found to be fairly similar in magnitude despite substantial regional differences in observed Apparent Effects. This may indicate that CMIP6 models are

This article is protected by copyright. All rights reserved.

Accepted Article

21698996, ja, Downloaded from https://agupubs.onlinelibrary.wiley.com/doi/10.1029/2021JD035476 by University Of Oslo Central 340, Wiley Online Library on [21/10/2022]. See the Terms and Conditions (https://onlinelibrary.wiley.com/terms-and-conditions) on Wiley Online Library for rules of use; OA articles are governed by the applicable Creative Commons License

unable to account for regional differences in aerosol effect on radiative transfer through the atmosphere. However, this presumes accurate input aerosol/precursor emissions.

More studies are necessary in order to fully uncover the mechanisms behind observed dimming and brightening. In particular, to further study the relative contribution from various emission species on the observed dimming/brightening trends, a multiple regression analysis could be carried out on observational data and emission inventories. This may also help uncover causes behind the continuing biases in ESM simulations.

A tough challenge in this field of study is the lack of data coverage and the necessity to use proxy measurements and synthetic data. Therefore, it is especially important to continually assess the data quality of observed radiation, clouds and aerosols. Furthermore, biases in ESM simulations of atmospheric effects on radiative fluxes remains an issue; in particular, the regionality of the ESM bias found here and in Moseid, et al. (2020) is a highly interesting discovery in this regard.

Open research

All datasets used in this study are currently available for download online via the links provided below. It should be noted that the authors cannot guarantee that these links are live in the future:

- ngGEBA (gap-filled version of GEBA) is available via the following link: dx.doi.org/10.5281/zenodo.4382033 (Storelvmo, 2020)
- CRU TS v4.02 and other versions of CRU are available on the website of the Climatic Research Unit at the University of East Anglia: crudata.uea.ac.uk/cru/data/hrg/ (East Anglia, 2020)
- CEDS anthropogenic emissions are available from https://doi.org/10.22033/ESGF/input4MIPs.1241 ("CMIP6 CEDS") (Hoesly, et al., 2017)) and https://zenodo.org/record/4025316 ("2020 CEDS") (O'Rourke, et al., 2020)
- CMIP6 gridded model output can be downloaded from esgf-node.llnl.gov/search/cmip6/ (World Climate Research Programme, 2020). For the same CMIP6 data studied herein, the following filters must be chosen: experiment ID: *historical*, variant label: *r1i1p1f1*, table ID: *Amon*, frequency: *mon*. The variables used in this study include: *rsdt*, *rsds*, *rsdscs* and *clt*.
- Figure 3: Decadal running average of the value of an unfixed Ecloudy as computed from multi-model mean in historical CMIP6 experiments, collocated to the ngGEBA stations in each region. In each legend item, the average of the respective region's Ecloudy trendline is printed.
-
- Figure 4: Anomalies of decadal running averages of (solid lines) no-cloud SSR computed using SSR from ngGEBA and cloud cover fraction from CRU TS v4.02 and various values for Ecloudy; (dotted, purple lines) all-sky SSR. Green is computed using regionally scaled values observed in Krakow, Poland; orange and yellow are computed using values computed from CMIP6 multi-model means (see Figure 2); in yellow, the unfixed values shown in Figure 2, in orange, the average value constant. All data is collocated to the ngGEBA stations in each region. The anomalies are computed by averaging the initial 5 years of the running mean time series, and subtracting this mean value from each time step.

This article is protected by copyright. All rights reserved.

Accepted Article

21698996, ja, Downloaded from https://agupubs.onlinelibrary.wiley.com/doi/10.1029/2021JD035476 by University Of Oslo Central 340, Wiley Online Library on [21/10/2022]. See the Terms and Conditions (https://onlinelibrary.wiley.com/terms-and-conditions) on Wiley Online Library for rules of use; OA articles are governed by the applicable Creative Commons License

Acknowledgments

The authors declare that they have no conflicts of interest.

The authors acknowledge valuable discussions with and input from Stein Julsrud, Erik Berge (The Norwegian Meteorological Institute) and Ian Harris (University of East Anglia).

The Global Energy Balance Archive (GEBA) is co-funded by the Federal Office of Meteorology and Climatology MeteoSwiss within the framework of GCOS Switzerland. Global dimming and brightening research at ETH Zürich is funded by the Swiss National Science Foundation (Grant No. 200020 188601).

This work was in part supported by European Union's Horizon 2020 research and innovation programme under grant agreement No 821205 (the FORCeS project).

This article is protected by copyright. All rights reserved.

Accepted Article

21698996, ja, Downloaded from https://agupubs.onlinelibrary.wiley.com/doi/10.1029/2021JD035476 by University Of Oslo Central 340, Wiley Online Library on [21/10/2022]. See the Terms and Conditions (https://onlinelibrary.wiley.com/terms-and-conditions) on Wiley Online Library for rules of use; OA articles are governed by the applicable Creative Commons License

Accepted Article

A Appendix

Table A shows the set of Earth system models analyzed in this study, along with their respective grid resolutions.

Table A: The 42 Earth System Models (ESMs) that are analysed in this study. All these ESMs participate in CMIP6 and have provided surface solar radiation, clear-sky surface solar radiation and cloud area fraction from the historical experiments. For each model, one ensemble member has been included in the analysis, r1i1f1p1.

ESM name	Nominal horizontal resolution	ESM name	Nominal horizontal resolution
CESM2-FV2	250 km	KIOST-ESM	250 km
CESM2-WACCM-FV2	100 km	MPI-ESM1-2-LR	250 km
FGOALS-g3	250 km	INM-CM4-8	100 km
E3SM-1-0	100 km	INM-CM5-0	100 km
FGOALS-f3-L	100 km	MPI-ESM-1-2-HAM	250 km
NESM3	250 km	IITM-ESM	250 km
SAM0-UNICON	100 km	MPI-ESM1-2-HR	100 km
BCC-CSM2-MR	100 km	AWI-ESM-1-1-LR	250 km
CanESM5	500 km	CMCC-CM2-HR4	100 km
MRI-ESM2-0	100 km	AWI-CM-1-1-MR	100 km
CESM2-WACCM	100 km	CMCC-CM2-SR5	100 km
CESM2	100 km	TaiESM1	100 km
MIROC6	250 km	IPSL-CM6A-LR	250 km
BCC-ESM1	250 km	ACCESS-CM2	250 km
E3SM-1-1	100 km	ACCESS-ESM1-5	250 km
ESM2-0	100 km	GFDL-ESM4	100 km
GISS-E2-1-G	250 km	NorESM2-LM	250 km
GISS-E2-1-H	250 km	NorESM2-MM	100 km
KACE-1-0-G	250 km	EC-Earth3	100 km
E3SM-1-1-ECA	100 km	EC-Earth3-Veg	100 km
CIESM	100 km	EC-Earth3-Veg-LR	250 km

This article is protected by copyright. All rights reserved.

21698996, ja, Downloaded from https://agupubs.onlinelibrary.wiley.com/doi/10.1029/2021JD035476 by University Of Oslo Central 340, Wiley Online Library on [21/10/2022]. See the Terms and Conditions (https://onlinelibrary.wiley.com/terms-and-conditions) on Wiley Online Library for rules of use; OA articles are governed by the applicable Creative Commons License

Accepted Article

B Appendix

Cloud cover data is utilized as input into the no-cloud SSR algorithm described in Section 2.4. However, the raw cloud cover data is not presented anywhere in the main text. Both observed (CRU TS v4.02) and multi-model mean (CMIP6) cloud cover is utilized to produce the results in the main text. Figure B shows anomaly plots of both the utilized timeseries of cloud cover for all four regions of focus in this study, with the base from which the anomaly is computed, printed in the legend items of the figure.

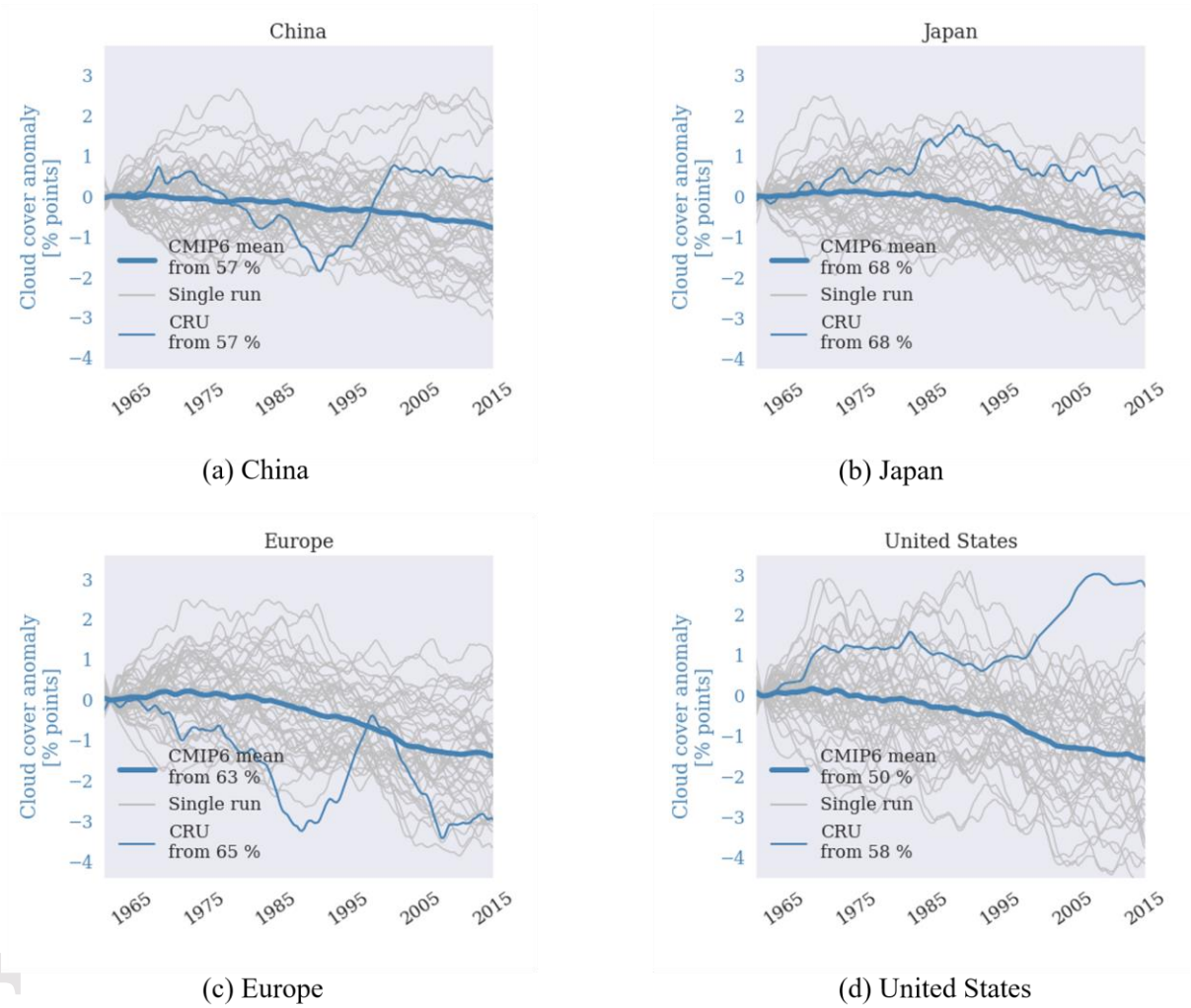

Figure B: Decadal running means of mean simulated (CMIP6) and observed (CRU TS v4.02) cloud cover percentage anomalies between 1961 and 2014 averaged over ngGEBA station locations in four regions: Multi-model mean CMIP6 in boldface and CRU TS v4.02 in lightface. Grey lines are decadal running means of each model run included. The anomalies are computed by averaging the initial 5 years of the running mean timeseries (this average is printed in the legend items, e.g., "from 57 %"), and subtracting this mean value from each subsequent time step. Included in the computation is one CMIP6 historical all-forcing simulation (r1i1f1p1) from each of the 42 models presented in Table A in Appendix A.

This article is protected by copyright. All rights reserved.

21698996, ja, Downloaded from https://agupubs.onlinelibrary.wiley.com/doi/10.1029/2021JD035476 by University Of Oslo Central 340, Wiley Online Library on [21/10/2022]. See the Terms and Conditions (https://onlinelibrary.wiley.com/terms-and-conditions) on Wiley Online Library for rules of use; OA articles are governed by the applicable Creative Commons License

Accepted Article

21698996, ja, Downloaded from https://agupubs.onlinelibrary.wiley.com/doi/10.1029/2021JD035476 by University Of Oslo Central 340, Wiley Online Library on [21/10/2022]. See the Terms and Conditions (https://onlinelibrary.wiley.com/terms-and-conditions) on Wiley Online Library for rules of use; OA articles are governed by the applicable Creative Commons License

References

Allen, R., Norris, J. & Wild, M., 2013. Evaluation of multidecadal variability in CMIP5 surface solar radiation and inferred underestimation of aerosol direct effects over Europe, China, Japan, and India. *Journal of Geophysical Research: Atmospheres,* 118(12), pp. 6311-6336.

Boucher, O., 2015. *Atmospheric Aerosols.* s.l.:Springer.

Boucher, O. et al., 2013. Clouds and aerosols. In: *Climate Change 2013: The Physical Science Basis. Contribution of Working Group I to the Fifth Assessment Report of the Intergovernmental Panel on Climate Change.* s.l.:Cambridge University Press, pp. 571-657.

Calbó, J. & Sanchez-Lorenzo, A., 2009. Cloudiness climatology in the Iberian Peninsula from three global gridded datasets (ISCCP, CRU TS 2.1, ERA-40). *Theoretical and applied climatology,* 96(1-2), pp. 105-115.

Cronin, T., 2014. On the choice of average solar zentih angle. *Journal of the Atmospheric Sciences,* 71(8), pp. 2994-3003.

East Anglia, U. o., 2020. *CRU TS v4.02 cloud cover data [Dataset]*. [Online]
Available at: https://crudata.uea.ac.uk/cru/data/hrg/
[Accessed 2020].

Eyring, V. et al., 2016. Overview of the Coupled Model intercomparison Prject Phase 6 (CMIP6) experimental design and organization. *Geoscientific Model Development,* pp. 1937-1958.

Forster, P. et al., 2021. The Earth's Energy Budget, Climate Feedbacks, and Climate Sensitivity. In: *Climate Change 2021: The Physical Science Basis. Contribution of Working Group I to the Sixth Assessment Report of the Intergovernmental Panel on Climate Change.* s.l.:Cambridge University Press.

Gilgen, H., Wild, M. & Ohmura, A., 1998. Means and Trends of Shortwave Irradiance at the Surface Estimated from Global Energy Balance Archive Data. *Journal of Climate,* 11(8), pp. 2042-2061.

Harris, I., Jones, P., Osborn, T. & Lister, D., 2014. Updated high-resolution grids of monthly climatic observations-the CRU TS3.10 Dataset. *International journal of climatology,* 34(3), pp. 623-642.

Harris, I. & Osborn, T., 2020. Version 4 of the CRU TS monthly high resolution gridded multivariate climate dataset. *Scientific data,* 7(1), pp. 1-18.

Hoesly, R. et al., 2017. *CMIP6 Forcing Datasets (input4MIPs) [Dataset]*. [Online]
Available at: https://doi.org/10.22033/ESGF/input4MIPs.1241

Hoyt, D. & Schatten, K., 1993. A discussion of plausible solar irradiance variations, 1700-1992. *Journal of Geophysical Research: Space Physics,* 98(A11), pp. 18895-18906.

Leirvik, T. & Yuan, M., 2021. A Machine learning technique for spatial interpolation of solar radiation observations. *Earth and Space Science,* 8(4).

Lewinschal, A. et al., 2019. Local and remote temperature response of regional SO2 emissions. *Atmospheric Chemistry and Physics,* Volume 19, pp. 2385-2403.

Liepert, B., 2002. Observed reductions of surface solar radiation at sites in the United States and worldwide from 1961 to 1990. *Geophysical Research Letters,* 29(10).

Liepert, B. & Kukla, G., 1997. Decline in Global Solar Radiation with Increased Horizontal Visibility in Germany between 1964 and 1990. *Journal of Climate,* 10(9), pp. 2391-2401.

Long, C. et al., 2009. Significant decadal brightening of downwelling shortwave in the continental United States. *Journal of Geophysical Research: Atmospheres,* 114(D10).

Matuszko, D., 2012. Influence of the extent and genera of cloud cover on solar radiation intensity. *International Journal of climatology,* 32(15), pp. 2403-2414.

This article is protected by copyright. All rights reserved.

Moseid, K. et al., 2020. Bias in CMIP6 models as compared to observed regional dimming and brightening. *Atmospheric Chemistry and Physics,* 20(24), pp. 16023-16040.
Myhre, G., Lund, C., Samset, B. & Storelvmo, T., 2013. Aerosols and their Relation to Global Climate and Climate Sensitivity. *Nature Education Knowledge,* 4(5), p. 7.
Naik, V. et al., 2021. Short-Lived Climate Forcers. In: *Climate Change 2021: The Physical Science Basis. Contribution of Working Group I to the Sixth Assessment Report of the Intergovernmental Panel on Climate Change.* s.l.:Cambridge University Press.
Norris, J. et al., 2016. Evidence for climate change in the satellite cloud record. *Nature,* 536(7614), pp. 72-75.
Norris, J. & Wild, M., 2009. Trends in aerosol radiative effects over China and Japan inferred from observed cloud cover, solar "dimming," and solar "brightening". *Journal of Geophysical Research: Atmospheres,* 114(D10).
Ohmura, A. & Lang, H., 1989. *IRS'88: Secular variation of global radiation in Europe.* Hampton, VA, A. Deepak Publ..
O'Rourke, P. R. et al., 2020. *CEDS Version comparison.* [Online]
Available at:
https://github.com/JGCRI/CEDS/blob/master/documentation/Version_comparison_figures_v_2020_09_11_vs_v_2016_07_16(CMIP6).pdf
[Accessed September 2020].
O'Rourke, P. R. et al., 2020. *CEDS v_2020_09_11 Pre-Release Emission Data [Dataset]*. [Online]
Available at: https://zenodo.org/record/4025316#.Y0MaULbP02w
[Accessed 2020].
Pfeifroth, U. et al., 2018. Trends and variability of surface solar radiation in Europe based on surface-and satellite-based data records. *Journal of Geophysical Research: Atmospheres,* 123(3), pp. 1735-1754.
Ramanathan, V., Crutzen, P., Kiehl, J. & Rosenfeld, D., 2001. Aerosols, Climate, and the Hydrological Cycle. *Science,* 294(5549), pp. 2119-2124.
Russak, V., 1990. Trends of solar radiation, cloudiness and atmospheric transparency during recent decades in Estonia. *Tellus B,* 42(2), pp. 206-210.
Schwarz, M. et al., 2020. Changes in atmospheric shortwave absorption as important driver of dimming and brightening. *Nature Geoscience,* Volume 13, pp. 110-115.
Smith, S. et al., 2015. *A Community Emissions Data System (CEDS): Emissions For CMIP6 and Beyond.* San Diego, CA, USA, s.n., pp. 12-16.
Stanhill, G. & Cohen, S., 2001. Global dimming: a review of the evidence for a widespread and significant reduction in global radiation with discussion of its probable causes and possible agricultural consequences. *Agricultural and Forest Meteorology,* 107(4), pp. 255-278.
Stanhill, G. & Kalma, J., 1995. Solar dimming and urban heating at Hong Kong. *International Journal of Climatology,* 15(8), pp. 933-941.
Stanhill, G. & Moreshet, S., 1994. Global radiation climate change at seven sites remote from surface sources of pollution. *Climatic Change,* Volume 26.
Storelvmo, T., 2020. *Gap filled GEBA data [Data set],* s.l.: Zenodo.
Storelvmo, T. et al., 2018. Lethargic response to aerosol emissions in current climate models. *Geophysical Research Letters,* 45(18), pp. 9814-9823.
Streets, D., Wu, Y. & Chin, M., 2006. Two-decadal aerosol trends as a likely explanation of the global dimming/brightening transition. *Geophysical Research Letters,* 33(15).
Swinehart, D., 1962. The Beer-Lambert Law. *Journal of Chemical Education,* 39(7), pp. 333-335.

This article is protected by copyright. All rights reserved.

Accepted Article

21698996, ja, Downloaded from https://agupubs.onlinelibrary.wiley.com/doi/10.1029/2021JD035476 by University Of Oslo Central 340, Wiley Online Library on [21/10/2022]. See the Terms and Conditions (https://onlinelibrary.wiley.com/terms-and-conditions) on Wiley Online Library for rules of use; OA articles are governed by the applicable Creative Commons License

Twomey, S., 1977. The influence of pollution on the shortwave albedo of clouds. *Journal of the atmospheric sciences,* 34(7), pp. 1149-1152.
Wang, K., Dickinson, R., Wild, M. & Liang, S., 2012. Atmospheric impacts on climatic variability of surface incident solar radiation. *Atmospheric Chemistry and Physics,* Volume 12, pp. 9581-9592.
Wang, Y. & Wild, M., 2016. A new look at solar dimming and brightening in China. *Geophysical Research Letters,* 43(22), pp. 11-777.
Wang, Z. L. L. X. Y. et al., 2021. Incorrect Asian aerosols affecting the attribution and projection of regional climate change in CMIP6 models. *npj Climate and Atmospheric Science,* 4(1), pp. 1-8.
Wild, M., 2009. Global dimming and brightening: A review. *Journal of Geophysical Research: Atmospheres,* 114(D10).
Wild, M., 2012. Enlightening global dimming and brightening. *Bulletin of the American Meteorological Society,* Volume 1, pp. 27-37.
Wild, M., 2016. Decadal changes in radiative fluxes at land and ocean surfaces and their relevance for global warming. *Wiley Interdisciplinary Reviews: Climate Change,* 7(1), pp. 91-107.
Wild, M. et al., 2017. The Global Energy Balance Archive (GEBA): A Database for the worldwide measured surface energy fluxes. *AIP Conf. Proc.,* 1810(090013).
Wild, M. & Schmucki, E., 2010. Assessment of global dimming and brightening in IPCC-AR4/CMIP3 models and ERA40. *Climate Dynamics.*
Wild, M. & Schmucki, E., 2011. Assessment of global dimming and brightening in IPCC-AR4/CMIP3 models and ERA40 based on surface observations. *Clim. Dyn.,* Volume 37, pp. 1671-1688.
Wild, M., Wacker, S., Yang, S. & Sanchez-Lorenzo, A., 2021. Evidence for Clear-Sky Dimming and Brightening in Central Europe. *Geophysical Research Letters,* Volume 48.
Willson, R. & Mordvinov, A., 2003. Secular total solar irradiance trend during solar cycles 21-23. *Geophysical Research Letters,* 30(5).
World Climate Research Programme, 2020. *CMIP6 Data search | ESGF-CoG [SearchEngine]*. [Online]
Available at: https://esgf-node.llnl.gov/search/cmip6/
[Accessed 2020].
Yang, S., Wang, X. & Wild, M., 2018. Homogenization and trend analysis of the 1958-2016 in situ surface solar radiation records in China. *Journal of Climate,* 31(11), pp. 4529-4541.
Yang, S., Wang, X. & Wild, M., 2019. Causes of dimming and brightening in China inferred from homogenized daily clear-sky and all-sky in situ surface solar radiation records (1958–2016). *Journal of Climate,* 32(18), pp. 5901-5913.
Zhao, T. et al., 2006. A Simulated Climatology of Asian Dust Aerosol and Its Trans-Pacific Transport. Part I: Mean Climate and Validation. *Journal of Climate,* 19(1), pp. 88-103.

This article is protected by copyright. All rights reserved.

Accepted Article

21698996, ja, Downloaded from https://agupubs.onlinelibrary.wiley.com/doi/10.1029/2021JD035476 by University Of Oslo Central 340, Wiley Online Library on [21/10/2022]. See the Terms and Conditions (https://onlinelibrary.wiley.com/terms-and-conditions) on Wiley Online Library for rules of use; OA articles are governed by the applicable Creative Commons License